Water Research 296 (2026) 125608

Contents lists available at ScienceDirect

Water Research

journal homepage: www.elsevier.com/locate/watres

Accumulation of recalcitrant dissolved organic matter during the formation of new North Pacific Intermediate Water in the Kuroshio-Oyashio confluence region

Lulu Han [a,b], Rong Huang [c], Ke Zeng [c], Xiao-Hua Zhang [b,c], Honghai Zhang [a], Zhaohui Chen [d], Peng Yao [a,b,*]

[a] Frontiers Science Center for Deep Ocean Multispheres and Earth System, and Key Laboratory of Marine Chemistry Theory and Technology, Ministry of Education, Ocean University of China, Qingdao 266100, China
[b] Laboratory for Marine Ecology and Environmental Science, Qingdao Marine Science and Technology Center, Qingdao 266237, China
[c] College of Marine Life Sciences, and Institute of Evolution and Marine Biodiversity, Ocean University of China, Qingdao 266100, China
[d] Physical Oceanography Laboratory, Ocean University of China, Qingdao 266100, China

HIGHLIGHTS

- The conservative composition of CDOM can be used to trace water mass mixing.
- The formation of new NPIW promotes the production of recalcitrant DOM.
- Microbial interactions during water mass mixing shape the alterations in DOM.

GRAPHICAL ABSTRACT

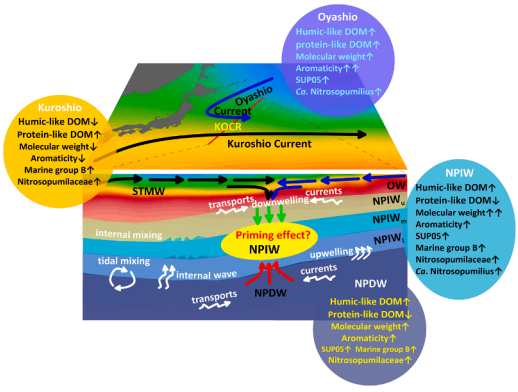

ARTICLE INFO

Keywords:
Kuroshio-Oyashio confluence region
North Pacific Intermediate Water
Recalcitrant dissolved organic matter
Chromophoric dissolved organic matter
Microbial interactions
Priming effect

ABSTRACT

Dissolved organic matter (DOM) represents the largest reservoir of reduced carbon in the oceans; however, the characteristic changes in DOM during oceanic dynamic mixing remain inadequately understood. This study examined the concentrations of dissolved organic carbon (DOC), the optical properties of chromophoric and fluorescent dissolved organic matter (CDOM and FDOM), and the composition of microbial communities in water samples collected in June 2022 from the Kuroshio-Oyashio confluence region of the northwest Pacific Ocean. A three end-member mixing model based on the conservative components of CDOM and neutral density was established to quantitatively differentiate the contributions of SubTropical Mode Water (STMW), Oyashio Water (OW), and North Pacific Deep Water (NPDW) to North Pacific Intermediate Water (NPIW). Building on this model, the variations in the sources and composition of DOM and the mechanisms governing these changes during water mass mixing in this region were investigated. The primary objective of this study was to examine

* Corresponding author.
E-mail address: yaopeng@ouc.edu.cn (P. Yao).

https://doi.org/10.1016/j.watres.2026.125608
Received 25 October 2025; Received in revised form 31 January 2026; Accepted 20 February 2026
Available online 21 February 2026

whether the mixing processes of water masses can promote the formation of refractory DOM (RDOM) and to assess the contribution of NPDW to the formation of NPIW and the transformation of DOM properties within it. The results indicated that, depending on the degree of water mass influence, NPIW can be further categorized into three sub-components: upper, middle, and lower NPIW. In the upper NPIW ($NPIW_u$), both humic-like and protein-like substances are consumed, with microorganisms such as *Ca.* Nitrosopumilus and SUP05 likely playing significant roles. In the middle NPIW ($NPIW_m$), in addition to the aforementioned processes, there is also an influence from deep-water microorganisms like Nitrosopumilaceae and Marine group B, leading to the accumulation of high molecular weight, more humified, and recalcitrant DOM (RDOM). In the lower NPIW ($NPIW_l$), *Ca.* Nitrosopumilus and other microorganisms gradually decline, leaving predominantly the influence of deep-water microorganisms, resulting in a continued accumulation of RDOM. The potential priming effects of microbial activity may play a crucial role in the transformation of DOM properties. This study enhances our understanding of the controls on the transport and transformation processes of DOM during water mass mixing, thereby contributing to our knowledge of the mechanisms underlying the production and persistence of RDOM in oceanic environments.

1. Introduction

The ocean serves as a significant carbon reservoir, absorbing carbon dioxide (CO_2) emissions from human activities and playing a crucial role in the global carbon cycle (Hansell et al., 2009). It stores approximately 685 petagrams of carbon (Pg C) in the form of dissolved organic carbon (DOC), which is roughly 200 times the total biomass of marine organisms and comparable to the atmospheric carbon pool (Sabine et al., 2004). In the global cycle of DOC, the vertical distribution of DOC is closely associated with ocean stratification, which is primarily influenced by ocean circulation processes (Wang et al., 2021b). Concurrently, various biological and chemical processes occur during the transport, mixing, and formation of water masses (Letscher et al., 2022; Kang et al., 2022; Gomez-Leton et al., 2022; Chang et al., 2024). Among these processes, the formation of marine intermediate water is a critical mechanism for the stabilization of dissolved organic matter (DOM) in the ocean (Talley, 1997; Swan et al., 2009; Catalá et al., 2016; Yamashita et al., 2017; Cao et al., 2020; Wang et al., 2021b; Liu et al., 2023). Furthermore, the microbial production of recalcitrant DOM (RDOM) is regarded as a critical factor driving long-term carbon storage in the global ocean (Jiao et al., 2014; Lechtenfeld et al., 2014; Xia et al., 2022; Xiao et al., 2023). Despite extensive research on the mechanisms underlying the production and persistence of marine RDOM (Zhao et al., 2024; Cai and Jiao, 2024), the characteristic changes in DOM during oceanic dynamic mixing, particularly their impact on the accumulation of RDOM, remain poorly understood.

The Kuroshio-Oyashio Confluence Region (KOCR) in the Northwest Pacific Ocean (NWPO) is one of the planet's most important oceanic carbon sinks (Takahashi et al., 2009), which is characterized by complex oceanic dynamic processes and active air-sea material exchange (Fig. 1a) (Ding et al., 2018; Gan et al., 2023). The mixing of the Kuroshio and Oyashio currents promotes the formation of North Pacific Intermediate Water (NPIW) (Yang et al., 2018), which plays a crucial role in ocean circulation and facilitates the transport of significant amounts of DOM into the deep ocean (Ge et al., 2022; Hansell et al., 2002). However, our understanding of the changes in the composition of DOM during the mixing processes of the Kuroshio and Oyashio Currents, as well as during the formation of NPIW, remains limited. For example, the mixing of the Kuroshio and the Oyashio Currents primarily occurs in water depths shallower than 200 meters (Takahashi et al., 2009). However, the remineralization of labile and semi-labile DOM predominantly occurs at the onset of NPIW formation (below 200 meters), while below 1000 meters, DOM primarily consists of RDOM following biodegradation (Williams and Druffel, 1987; Hansell et al., 2009; Hansell and Carlson, 2013; Medeiros et al., 2015; Cao et al., 2020). This indicates that the transformation of DOM properties may not primarily occur during the mixing of the Kuroshio and Oyashio Currents, but rather during the formation and transport processes of NPIW. Investigating whether the mixing processes of water masses promote the accumulation of RDOM is crucial for understanding the mechanisms

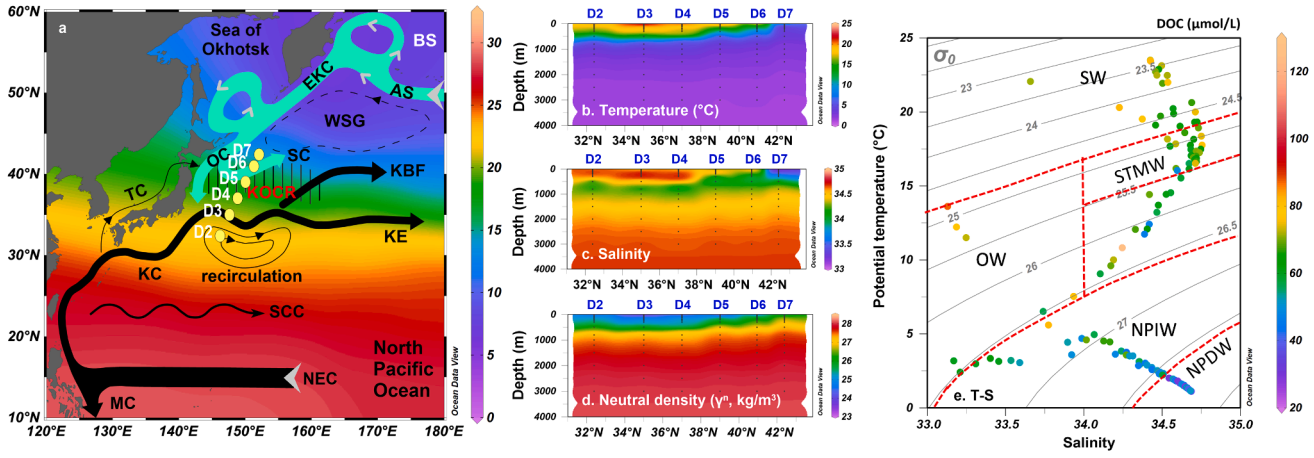

Fig. 1. (a) Location of sampling sites in the Kuroshio-Oyashio confluence region (KOCR) of the northwest Pacific Ocean; profiles of (b) Temperature, (c) Salinity, and (d) Neutral density (γ^n); (e) Potential temperature-salinity (T-S) diagram. The color bar indicates dissolved organic carbon (DOC) concentrations, and the grey lines represent potential density anomaly (σ_0). The red dotted lines represent the classification of water masses based on salinity, potential temperature, depth, and σ_0. The ocean currents are as follows: Kuroshio Current (KC), Oyashio Current (OC), Kuroshio Extension (KE), Subtropical Countercurrent (SCC), North Equatorial Current (NEC), Mindanao Current (MC), Kuroshio Bifurcation Front (KBF), Western Subarctic Gyre (WSG), Subarctic Current (SC), East Kamchatka Current (EKC), Alaskan Stream (AS), Bering Sea (BS), and Tsushima Current (TC). The water masses are as follows: Surface Water (SW), SubTropical Mode Water (STMW), Oyashio Water (OW), and North Pacific Deep Water (NPDW), North Pacific Intermediate Water (NPIW).

underlying the formation and persistence of RDOM in the ocean. Previous studies have largely approached the formation of oceanic RDOM as a conceptual model or through laboratory incubation experiments (Jiao et al., 2011; Arrieta et al., 2015; Shen and Benner, 2020; Dittmar et al., 2021). In addition, in traditional models of water mass mixing, the upper NPIW, also referred to as new NPIW, is primarily thought to arise from the mixing of the Kuroshio and Oyashio Currents, while the lower NPIW, or old NPIW, is predominantly influenced by subtropical mode water (STMW) (Yoshinari et al., 2001). Based on this understanding, Talley (1997) calculated that 55% of new NPIW originates from the Kuroshio Current and 45% from the Oyashio Current. Other studies related to water mass mixing have also assumed that NPIW is formed solely from the mixing of these two currents (Yasuda et al., 1996; Hansell et al., 2002; Shin-ichi et al., 2017). Nevertheless, increasing evidence suggests that North Pacific Deep Water (NPDW) also contributes to the formation of NPIW (Gong et al., 2019). However, the extent to which NPDW influences the transformation of DOM properties during the formation of NPIW remains poorly understood.

Chromophoric dissolved organic matter (CDOM), which includes fluorescent dissolved organic matter (FDOM), constitutes a significant component of DOM in aquatic environments (Martínez-Pérez et al., 2017; Chen et al., 2019; D'Andrilli et al., 2022). The sources, composition, distribution, and transformation of CDOM directly influence the OC cycle in oceanic waters, making it an essential element of the global carbon cycle (Shields et al., 2019; Kim et al., 2022; An et al., 2023; Álvarez et al., 2023; Meilleur et al., 2023). In particular, previous studies have shown that RDOM as traced by optical proxies such as humic-like FDOM is ubiquitous and accumulates in the dark ocean (Yamashita and Tanoue, 2008; Catalá et al., 2015; Wang et al., 2021a). However, investigations of CDOM in the global surface ocean indicate that the proportion of humic-like substances can vary by over 70% in different regions, which suggests significant spatial variability in the distribution of CDOM across the global ocean and underscores the distinct characteristics of various water masses (Catalá et al., 2016; Yamashita et al., 2017). The specific characteristics of CDOM in various water masses have been employed to differentiate among these water masses, including the KOCR (Chen and Gardner, 2004; Yamashita and Tanoue, 2009; Matsuoka et al., 2012, 2016; D'Sa et al., 2014; Gonçalves-Araujo et al., 2016; Tanaka et al., 2016; Mizuno et al., 2018; Yamashita et al., 2019; Hirawake et al., 2021). Water mass classification based on CDOM is often conducted by selecting conserved substances within CDOM and combining them with similarly conservative physical properties, such as salinity, to create an end-member model (Wang et al., 2022b). However, salinity is not always a reliable indicator for differentiating water masses. However, the salinity levels of STMW and NPDW are similar, making salinity an inadequate parameter for distinguishing the contributions of these two water masses. Neutral density, a measure of water density, is frequently used to differentiate water masses (Jackett and Mcdougall, 1997). In the NWPO, there is a significant difference in neutral density between surface Kuroshio and Oyashio waters and deep-water masses, allowing for effective differentiation (Sonnerup et al., 1999; Ganachaud, 2003; Swan et al., 2009). By integrating the conservative parameters of CDOM with neutral density, it may be possible to develop an end-member model that quantitatively distinguishes the contributions of different water masses more effectively. Furthermore, current research primarily focuses on tracing CDOM without adequately utilizing its semi-quantitative properties to explore the biogeochemical processes of DOM during water mass mixing. The development of a robust model would facilitate a more comprehensive investigation of the changes in DOM during the water mass mixing process.

In this study, the concentrations of DOC, the optical properties—including ultraviolet-visible absorption of CDOM and three-dimensional fluorescence spectral characteristics of FDOM, and the composition of microbial communities based on 16S rDNA analysis were determined in water samples collected from the KOCR in June 2022. Using the conservative components of CDOM and the neutral density as source markers, a mixing model was established to differentiate the proportions of water masses. The changes in the non-conservative components of DOM during the mixing process were calculated by utilizing the difference between the measured values and the theoretical mixing values derived from model results. Building on these calculations, the variations in the sources and composition of DOM, as well as the primary mechanisms that control these changes during water mass mixing, particularly in the context of NPIW formation in this region were investigated. The overarching objective of this study was to examine whether the mixing processes of water masses can promote the formation of RDOM and to assess the contribution of NPDW to the formation of NPIW and the transformation of DOM properties within it. The findings of this study will fill the knowledge gaps regarding the controls on the transport and transformation processes of DOM during water mass mixing, and will enhance our understanding of the mechanisms that govern the production and persistence of RDOM in oceanic environments.

2. Materials and methods

2.1. Study area and sampling

The Kuroshio Current originates in the southern subtropical Pacific and flows northward, characterized by warm, saline waters but low nutrient levels (Fig. 1a) (Talley, 2011; Long et al., 2018). During its northeastward flow, the Kuroshio Current experiences a gradual decrease in temperature and descends, forming a mode water mass between 20° and 35°N, known as STMW (Suga and Hanawa, 1990; Bingham et al., 1992; Qu et al., 2002; Oka and Qiu, 2012; Wang et al., 2022a; Ju et al., 2025). In contrast, the Oyashio Current originates in the subarctic region and flows southward, featuring colder and less saline water that is rich in nutrients (Fig. 1a) (Talley, 2011; Long et al., 2019). The initial mixed water body formed by the confluence of the Kuroshio and Oyashio currents is replenished into the NPIW, commonly referred to as new NPIW or upper NPIW, and contributing to the widespread distribution of NPIW in the NWPO (Yasuda et al., 1996; Masujima and Yasuda, 2009). The NPIW typically resides at depths between 200 and 1500 meters; deeper than this, North Pacific Deep Water (NPDW) does not form locally but instead represents the oldest water mass in the world, which ascends to contribute to the formation of NPIW while simultaneously transporting materials to the lower NPIW through vertical advection (Fig. 1a) (Talley, 1997; Hansell et al. 2002; Medeiros et al. 2015). In addition, factors that may promote mixing include lateral transport, tidal mixing (which generates internal waves), and internal mixing (Talley, 1997; Masunaga et al., 2019).

In June 2022, a total of 126 seawater samples were collected from six stations located between 146.19°E to 152.03°E and 32.39°N to 42.39°N, at depths ranging from 5 m to 4000 m on board the R/V Dongfanghong 3 (Fig. 1a). The vessel is equipped with a rosette system that includes a Seabird 911 CTD (conductivity, temperature, and depth) profiler and 24-liter Niskin bottles, capable of simultaneously measuring salinity, temperature, and depth during sampling operations. The potential temperature is the temperature at which the water is adiabatically adjusted to the surface pressure (Broecker et al., 1985). The potential density anomaly (σ_0) was calculated based on the measured values of salinity, temperature, and depth. The calculation of σ_0 involves the influence of depth; however, during the global water cycle, there are multiple instances of vertical overturning. To relate the water masses before and after these overturns, neutral density (γ^n) was calculated based on σ_0, which effectively eliminates the influence of depth while retaining the effects of temperature and salinity (Jackett and Mcdougall, 1997). This approach allows for a more effective distinction of water masses compared to using σ_0 alone.Upon collection, the water samples for DOC and CDOM analyses were immediately filtered through pre-combusted (at 450°C) glass fiber filter membranes (Whatman GF/F,

0.7 μm pore size). The water samples for DOC and CDOM analysis, were stored at -20°C until further analysis (Spencer and Coble, 2014). Additionally, samples for microbial analysis were filtered using polycarbonate filter membranes (Isopore, 0.2 μm pore size) and were stored at -80°C prior to laboratory analysis.

2.2. Analysis of the concentration and optical properties of DOM

The DOC concentration was determined using a Shimadzu TOC-L CPH analyzer, with the pH of the samples adjusted to 2 (Guo et al., 1995). The deep-sea water reference obtained from the Hansell Biogeochemical Laboratory at the University of Miami, USA, was utilized as a standard for measurement validation. The analytical uncertainty for DOC in duplicate samples was < 3% (n=8). The UV-Vis properties were assessed using a Shimadzu UV-2700i dual-beam spectrophotometer, which operated over a wavelength range of 200 to 800 nm, utilizing a 10-cm quartz cuvette at room temperature (Kakehi et al., 2017). The fluorescence properties were measured using a Shimadzu RF-6000 fluorescence spectrophotometer, with excitation wavelengths ranging from 240 to 450 nm in 5 nm increments and emission wavelengths spanning from 250 to 550 nm in 1 nm increments (Lawaetz and Stedmon, 2009). A Milli-Q water blank was added to every six samples during the measurement of CDOM and FDOM to perform blank corrections and monitor the instrument's status and stability.

Several optical parameters were calculated to characterize CDOM (FDOM), including the absorbance coefficient at 254 nm (a_{254}), specific UV–visible absorbance at 254 nm ($SUVA_{254}$), the spectral slope from 275 nm to 295 nm ($S_{275\text{-}295}$), the humification index (HIX), and the biological index (BIX) (Ohno, 2002; Weishaar et al., 2003; Helms et al. 2008; Huguet et al., 2009; Martínez-Pérez et al. 2017). Please refer to the Supporting Material for the definitions and calculation methods of each CDOM parameter.

Additionally, parallel factor analysis (PARAFAC) was conducted based on fluorescence excitation-emission matrix (EEM) spectroscopy to resolve the various components of FDOM using Matlab 2022b (Math Works) (Murphy et al., 2011). The FDOM components identified by the EEM-PARAFAC method were compared with the OpenFluor spectra database (lablicate.com), yielding statistical matches with previous studies at a confidence level of > 95% (Murphy et al., 2014).

2.3. Analysis of the microbial species and abundance

DNA information from the samples was obtained through processes including extraction, separation, amplification, purification, and sequencing, which were subsequently converted into species information and abundance (Huang et al., 2026). In brief, the primers commonly used for bacteria and archaea, 515FmodF and 806RmodR, were employed to amplify the highly variable V4 region of the 16S rRNA gene. Following Illumina sequencing, paired-end reads were processed to split the samples. Initially, the paired-end reads underwent quality control and filtering based on sequencing quality using fastp (version 0.19.6). Subsequently, the reads were merged using FLASH (version 1.2.7) based on their overlap, resulting in a total of 34,402,386 quality-controlled and merged reads with an average length of 253 bp. The optimized data were then processed using the DADA2 sequence denoising method to obtain Amplicon Sequence Variants (ASVs) along with their abundance information. Taxonomic classification was performed using the RDP classifier (version 11.5, https://sourceforge.net/projects/rdp-classifier/) with a confidence threshold set at 70%. The classification was conducted by comparing the 16S rDNA sequences against the Silva138 16S database (https://www.arb-silva.de/) using the classify-sklearn (Naive Bayes) approach. Please refer to the Supporting Material for detail microbial analysis methods.

2.4. Model calculations and statistical analysis

A three end-member mixing model based on a Monte-Carlo simulation approach using γ^n and the conservative component of FDOM (C3) as source markers was employed to distinguish the relative contributions of STMW, Oyashio Water (OW) and NPDW to the NPIW (Andersson et al., 2015; Zhao et al., 2021). In the Monte-Carlo simulation strategy, end-member values were assumed to follow a normal distribution within the given mean and standard deviation (Andersson, 2011). The Monte-Carlo simulation was executed using a modified MATLAB script (Version R2023b, Math Works) (Andersson et al., 2015). For each sample, 1,000,000 out of 100,000,000 random samples from the normal distribution of each end-member were taken to simultaneously fulfill the given system (Eqs. 1-3). The mean relative contributions and the standard deviation of three water masses were then calculated for each sample from the MC simulation solutions. Variations in mean relative contributions for end-members of a given sample were all less than 0.1%, and were determined by randomly sampling each parameter value 7 times, ensuring the statistical stability of the model.

$$Y_{sample} = f_{STMW} \times Y_{STMW} + f_{OW} \times Y_{OW} + f_{NPDW} \times Y_{NPDW} \quad (1)$$

$$C_{sample} = f_{STMW} \times C_{STMW} + f_{OW} \times C_{OW} + f_{NPDW} \times C_{NPDW} \quad (2)$$

$$f_{STMW} + f_{OW} + f_{NPDW} = 1 \quad (3)$$

where, Y_{sample} represents the γ^n values of samples in mixed waters; Y_{STMW}, Y_{OW} and Y_{NPDW} are the end member values of γ^n for STMW, OW and NPDW, respectively (Fig. 5a). These values were derived by averaging the γ^n data from samples within each water mass, with the range of variation defined as one standard deviation. C_{sample} denotes the concentrations of C3 component of samples in mixed waters; C_{STMW}, C_{OW} and C_{NPDW} are the end member values of C3 concentration for STMW, OW and NPDW, respectively (Fig. 5a). The methods used to obtain these values are consistent with those described previously.

It is important to note that the classification of samples of each end-member water mass and NPIW is primarily based on γ^n, while also incorporating salinity and σ_0. According to the definition of water masses in Pacific Ocean by γ^n in previous studies, the STMW (25.0 kg m^{-3}≤γ^n≤25.8 kg m^{-3}), NPIW (26.0 kg m^{-3}≤γ^n≤27.4 kg m^{-3}) and NPDW (27.8 kg m^{-3}≤γ^n≤28.1 kg m^{-3}) all fall within the range of γ^n of samples in this study (Sonnerup et al., 1999; Ganachaud, 2003; Swan et al., 2009). However, calculations revealed that the σ_0 of samples with γ^n ranging from 27.4 to 27.8 kg m^{-3} falls between 26.6 and 27.6 kg m^{-3} (Fig. 1e). According to the definition of NPIW based on potential density, these samples also qualify as NPIW (Talley, 1997). Therefore, in this study, we define this subset of samples also as NPIW. In addition to meeting the criteria for neutral density, STMW samples must also have a salinity greater than 34 (Long et al., 2018). In contrast, OW does not have a defined neutral density and is characterized by a salinity of less than 34 at depths between 50 and 150 meters (Long et al., 2019). In addition, surface water (SW) was excluded from the model. The SW refers to the water layer situated above the STMW and the OW, which is primarily characterized by the exchange of materials between the ocean surface and the atmosphere (Fig. 1e).

Subsequently, changes in other DOM parameters associated with biogeochemical processes were calculated by subtracting the theoretical values from the measured values. The details of the calculation are as follows:

$$X_m = f_{STMW} \times X_{STMW} + f_{OW} \times X_{OW} + f_{NPDW} \times X_{NPDW} \quad (4)$$

$$\Delta X = X_{sample} - X_m \quad (5)$$

where, X_m represents the theoretical values of non-conservative parameters of DOM in mixed waters, derived from the linear mixing of STMW, OW, and NPDW. X_{STMW}, X_{OW} and X_{NPDW} are the mean values of samples within each of the three aforementioned water masses. X_{sample}

represents the measured values of non-conservative parameters of dissolved organic matter (DOM) in mixed waters, while ΔX denotes the difference between the theoretical mixing values and the observed values. This difference reflects the biogeochemical changes in non-conservative parameters of DOM resulting from the mixing processes of water masses.

Statistical calculations and analyses were performed using OriginPro 2024b and MATLAB 2022b. Pearson correlation and principal component analysis (PCA) were conducted based on data pertaining to salinity, optical parameters of DOM, DOC concentrations, and microbial communities at the genus level (Yao et al., 2015). A significance threshold of $p < 0.05$ was established for all statistical analyses.

3. Results

3.1. Hydrological characteristics

The salinity of all samples ranged from 33.1 to 34.8, with a mean of 34.4 (Fig. 1b). With the exception of a few samples, all salinity values exceeded 34 (Fig. 2a). The temperature values varied from 1.4°C to 23.5°C (Fig. 1c), reflecting the collection of samples across approximately 10 degrees of latitude and a depth of 4000 meters. The γ^n increased from 23.2 to 28.1, exhibiting a trend of increasing from top layer to bottom and from south to north, which corresponds to the distributions of temperature and salinity (Fig. 1d).

3.2. DOC concentration and optical properties of DOM

DOC concentrations for all samples analyzed ranged from 28.9 to 124.3 μmol L^{-1}, with a mean of 59.1 ± 13.8 μmol L^{-1}. The mean DOC concentrations, from surface to deeper layers, were as follows: 70.9 ± 6.4 μmol L^{-1} in SW, 64.7 ± 6.8 μmol L^{-1} in STMW, 61.0 ± 1.3 μmol L^{-1} in OW, 57.0 ± 14.1 μmol L^{-1} in NPIW, and 42.2 ± 7.4 μmol L^{-1} in NPDW, similar with previous studies (Figs. 2a and S2a) (Ge et al., 2022; Wang et al., 2022b). DOC concentrations decreased with depth, reaching a minimum in the NPDW. The a_{254}, which indicates the concentration of more reactive CDOM, ranged from 0.6 to 2.1 m^{-1}, with a mean of 1.1 ± 0.2 m^{-1}. The mean a_{254} values in the SW, STMW, OW, NPIW, and NPDW waters are 1.2 ± 0.2 m^{-1}, 1.1 ± 0.2 m^{-1}, 1.7 ± 0.2 m^{-1}, 1.1 ± 0.2 m^{-1}, and 0.9 ± 0.1 m^{-1}, respectively (Figs. 2b and S2b). In SW and STMW, the concentration of CDOM is slightly lower and the concentration of DOC is higher, while in other water masses, the variations in CDOM and DOC are generally consistent (Figs. 2a, b and S2a, b).

The $SUVA_{254}$ was highest in the OW, followed by the NPDW and NPIW, while the STMW and SW exhibited similar and lower values (Fig. 2c and S2c). The $S_{275\text{-}295}$ ranged from 8.8 to 40.0 μm^{-1}, with a mean of 20.8 ± 6.4 μm^{-1}. The $S_{275\text{-}295}$ values were observed in the following order from highest to lowest: SW, STMW, OW, NPIW and NPDW (Figs. 2d and S2d). The HIX values ranged from 0.32 to 1.00, with a mean of 0.70 ± 0.20. The HIX values were recorded as follows: SW (0.46 ± 0.09), STMW (0.58 ± 0.06), OW (0.58 ± 0.02), NPIW (0.85 ± 0.13), and NPDW (0.90 ± 0.06), indicating an increasing trend from surface to bottom (Figs. 2e and S2e). The BIX ranged from 0.45 to 0.69, with a mean of 0.52 ± 0.04. The BIX values were highest in SW (0.54 ± 0.0.04) and STMW (0.55 ± 0.02), followed by OW (0.53 ± 0.01), NPIW (0.50 ± 0.03), and NPDW (0.47± 0.01) (Figs. 2f and S2f).

Three components of FDOM were identified, of which Component 1 (C1) consists of a mixture of traditional humic-like peaks A and C (Fig. S1a) (Guéguen et al., 2014; Kothawala et al., 2014), while Component 2 (C2) is characterized by protein-like fluorescence (Guéguen et al., 2014; Kothawala et al., 2014; Catalá et al., 2015) (Fig. S1b). Component 3 (C3) is not fully characterized but displays both tryptophan-like and marine humic-like fluorescence characteristics; however, it is generally a more conservative fluorescent component compared to C1 and C2 (Fig. S1c) (Murphy et al., 2011; Catalá et al., 2015). C1 values ranged from 0.37 × 10^{-2} to 3.19 × 10^{-2} Raman Units (R. U.) (Fig. S2g). C1 were highest in OW, followed by NPIW, NPDW and STMW, and lowest in SW (Fig. 2). C2 values ranged from 0 to 3.42 × 10^{-2} R.U., exhibiting an inverse trend compared to C1, except in OW (Fig. S2h). C2 were highest in OW, followed by SW and STMW, and lowest in NPIW and NPDW (Figs. 2h). The differing consumption and formation processes of C1 and C2 in SW, STMW, and OW contribute to the inconsistent distribution of CDOM and DOC in the upper water layers. C3 values ranged from 0.21 × 10^{-2} R.U. to 3.12 × 10^{-2} R.U. (Figs. S2i). There was greater variability observed in the SW and NPIW waters, while the values remained more stable in the OW, STMW, and NPDW (Figs. 2i).

3.3. Microbial species and abundance

The results of the microbial community analysis indicate that the microorganisms in the KOCR exhibit a rich diversity, with a total of 1467 genera identified. However, the majority of these genera have low abundance. In this study, we selected the top 30 microbial genera based

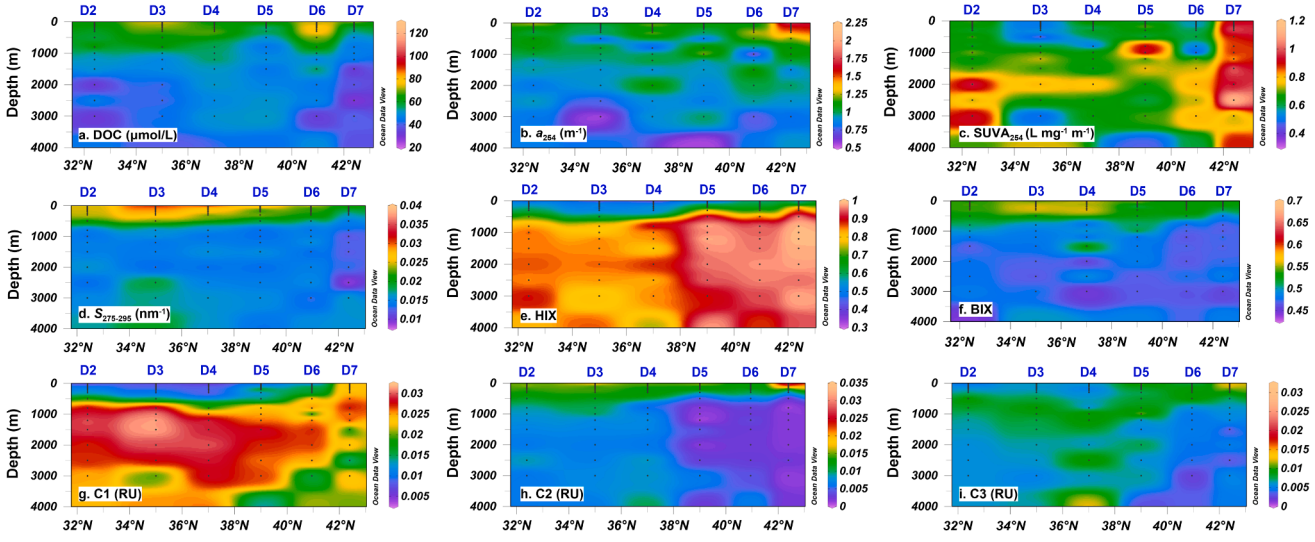

Fig. 2. Profiles of (a) DOC, (b) a_{254}, (c) $SUVA_{254}$, (d) $S_{275\text{-}295}$, (e) BIX, (f) HIX, (g) CDOM component C1, (h) C2, and (i) C3 in the KOCR of the northwest Pacific Ocean.

on their relative abundance for further analysis. The combined contribution of these 30 genera to the microbial abundance across all samples averaged over 70%, indicating that they can effectively represent the microbial community composition.

There are significant differences in the dominant microbial groups among different water masses and water layers. Among the identified microbial taxa, *Candidatus (Ca.)* Nitrosopelagicus was predominantly found in the STMW and exhibited very low abundance in the NPIW (Figs. 3a and S3a). Aegean-169 (no rank) was mainly distributed in the surface layer but was not restricted to this layer, extending down to depths below 2000 meters, with higher abundance observed in STMW compared to OW (Figs. 3b and S3b). *Ca.* Nitrosopumilus and an unclassified Nitrosopumilaceae primarily occurred in the upper layers of NPIW, with abundance increasing closer to the Oyashio Current (Figs. 3c and S3c). SUP05 and the Sva0996 marine group were widely distributed in the 300-1500 m depth range across stations D2-D5, while their distribution in stations D6 and D7 extended from 100 to 2000 m (Figs. 3d and S3d). An no rank Nitrosopumilaceae (hereafter referred to as Nitrosopumilaceae) were mainly found in waters below 150 m, particularly abundant at all stations deeper than 500 m (Figs. 3e and S3e). Marine group B (no rank) was broadly distributed across all samples but showed particularly high abundance in the mid-water layers, with significantly greater presence in STMW compared to OW (Figs. 3f and S3f).

3.4. Water mass classification based on end-member mixing model

In this study, a three end-member mixing model was established using γ^n and the conservative FDOM component C3 to calculate the contributions of STMW, OW, and NPDW during the formation of NPIW (Fig. 4a). The values of C3 and γ^n for STMW are relatively low, while OW exhibits higher C3 values and moderate γ^n. In contrast, NPDW demonstrates higher γ^n and lower C3. Except for a few stations at deeper depths, data from NPIW indicate that it can be formed by the mixing of STMW, OW, and NPDW (Fig. 4a).

The model results reveal that the contribution of STMW to NPIW decreases progressively from top to bottom and diminishes from the KOCR towards both the northern and southern sides (Fig. 4c). Notably, the upper layers of D3, D5, and D6 can reach up to 60%, a result consistent with previous studies reporting that the Kuroshio current accounts for 45% to 55% of the mixed layer (Talley, 1997). Below 1000 meters, the contribution is generally less than 10% (Fig. 4c). The influence of OW on NPIW varies with the sinking or rising of OW. In the KOCR, the sinking position of OW is deeper due to strong hydrodynamic conditions, resulting in a greater contribution. For example, significant influence regions greater than 50% are observed at depths of 250 m and 500 m at station D6, as well as at 500 m at station D2 (Fig. 4d). Overall, the contribution of OW to NPIW decreases gradually from the upper layers to the deeper layers. NPDW differs from OW and STMW in that its influence on NPIW is primarily from below. At the same depth, the northern region is more significantly affected by NPDW than the southern region (Fig. 4e). Therefore, based on the predominant influencing water masses, NPIW can be further divided into three sub-components: (1) $NPIW_u$, which is concentrated in the upper southern layer and is primarily influenced by STMW, with f_{STMW} exceeding 30%. Except for samples from station D6 at depths of 150 m and 175 m, all other samples in $NPIW_u$ show f_{STMW} greater than f_{OW}; (2) $NPIW_m$, located in the upper northern layer, is primarily influenced by OW, with f_{OW} exceeding 30%, and f_{OW} also greater than f_{STMW}; (3) $NPIW_l$, which is concentrated in the deeper layer, is mainly influenced by NPDW, with the influences of STMW and OW both being less than 30% (Fig. 4b). Specifically, in $NPIW_u$, the proportions of STMW, NPDW, and OW are 49%, 30%, and 21%, respectively. In $NPIW_m$, the proportions are 16%, 44%, and 40%, while in $NPIW_l$, the proportions are 7%, 14%, and 79%, respectively.

3.5. PCA results

PCA was conducted on 126 samples based on 12 variables, including DOC concentration, CDOM parameters (a_{254}, $SUVA_{254}$, C1, C2, C3, $S_{275-295}$, BIX, and HIX), as well as basic hydrological parameters (salinity, temperature, and neutral density) (Fig. S4). Principle component 1

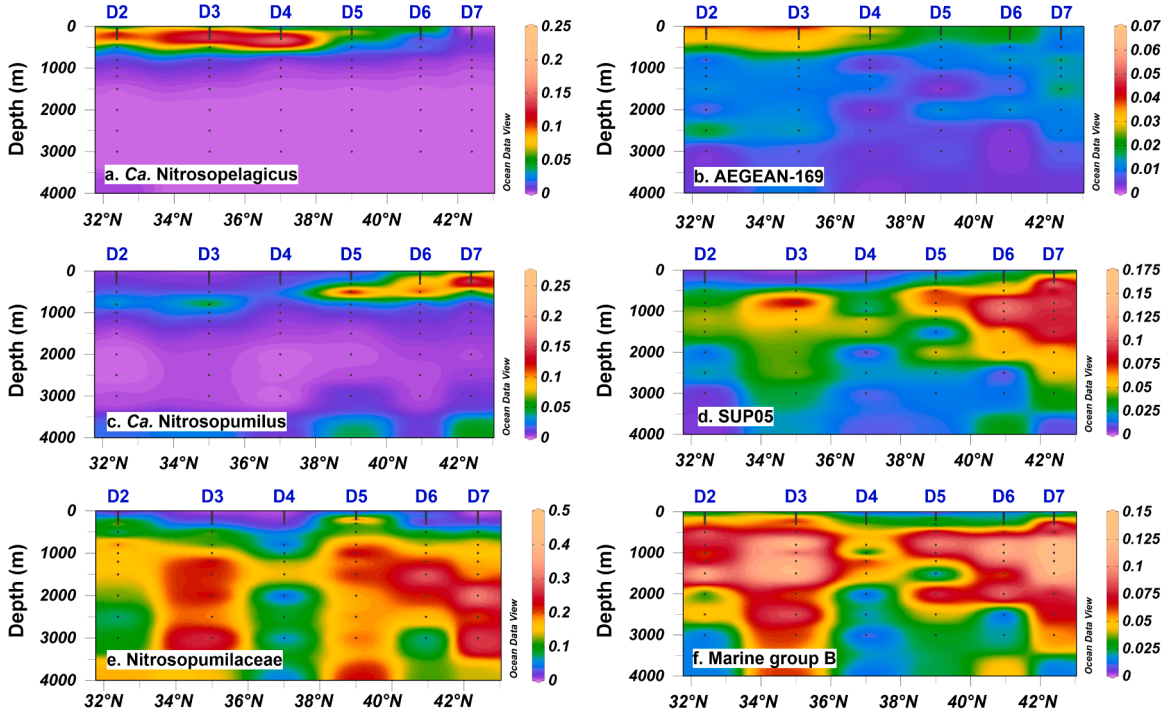

Fig. 3. Profiles of representative microbial communities, including (a) *Candidatus* Nitrosopelagicus, (b) Aegean-169, (c) *Candidatus* Nitrosopumilus, (d) SUP05, (e) Nitrosopumilaceae, and (f) Marine group B in the KOCR of the northwest Pacific Ocean.

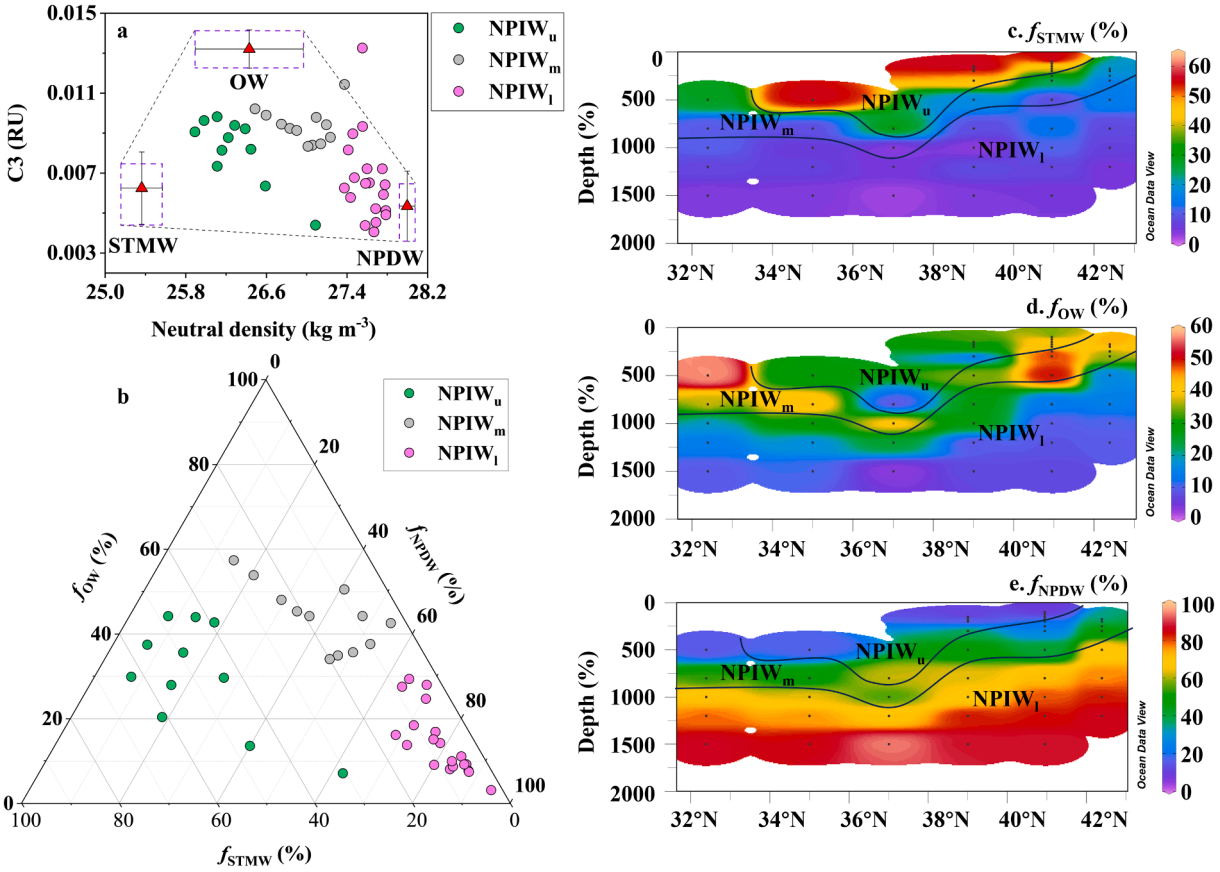

Fig. 4. (a) Scatter plots of the CDOM component C3 vs. neutral density (γ^n) of the North Pacific Intermediate Water (NPIW). The red triangles are endmember values of the water masses of SubTropical Mode Water (STMW), Oyashio Water (OW), and North Pacific Deep Water (NPDW). The error bars show the standard deviation of the endmember values. The green, grey and pink circles represent the samples of the upper, middle and lower sub-components of NPIW (NPIW$_u$, NPIW$_m$ and NPIW$_l$). (b) Ternary diagram of the contributions of STMW (f_{STMW}), OW (f_{OW}) and NPDW (f_{NPDW}) to NPIW. Profiles of the contributions of (c) STMW, (d) OW and (e) NPDW to NPIW in the KOCR of the northwest Pacific Ocean.

(PC1) and PC2 account for 53.5% and 21.9% of the total variance matrix, respectively. PC1 exhibits a strong positive variable loading with respect to temperature, DOC and CDOM concentrations, as well as the composition and properties associated with the production of low molecular weight CDOM (LMW CDOM) (BIX, C2, and C3). Conversely, it shows a significant negative loading concerning the γ^n and the composition and properties of refractory CDOM ($SUVA_{254}$, HIX, and C1). There is no variable loading related to salinity. The primary variables associated with the positive loadings of PC2 are γ^n, DOC and CDOM concentrations, and certain properties of CDOM ($SUVA_{254}$ and BIX). The most significant variable for the negative loadings of PC2 is salinity, along with temperature, $S_{275\text{-}295}$, and HIX.

Based on the sample scores, the sample points exhibit distinct regional delineations in the PCA (Fig. S4), which align closely with traditional physical oceanographic classifications. Different water masses are clearly represented in separate regions along the PC1 and PC2 axes. From right to left on the PC1 axis, the sequence is as follows: SW/STMW, OW, NPIW$_u$/NPIW$_m$, NPIW$_l$, and NPDW. Although SW/STMW and NPIW$_u$/NPIW$_m$ cannot be entirely separated along the PC1 axis, they can be distinctly differentiated along the PC2 axis. The observed increase in humification and decrease in freshness, as described in Section 3.2, corresponds negatively with the PC1 axis distribution. Additionally, the lower salinity of OW and NPIW$_m$ compared to other water masses is clearly indicated on the PCA as a shift in position along the PC2 axis. The PCA plot also illustrates the mixing processes of water masses: NPIW$_u$ is positioned at the angle formed by the line connecting OW and STMW, while NPIW$_m$ is located closer to OW and moving towards NPDW, with NPIW$_l$ situated nearer to NPDW.

4. Discussion

4.1. Tracking water masses mixing using the conservative components of FDOM and neutral density

The changes in the physicochemical properties of the water indicate significant mixing of water masses in the KOCR, which facilitates the formation of NPIW. As previously mentioned, some samples exhibit lower salinity levels; specifically, the few samples with salinity values below 34 are indicative of OW that is significantly influenced by terrigenous inputs (Talley, 2011; Long et al., 2019), as well as some NPIW samples that are predominantly composed of OW (Fig. 1b). As illustrated in Figs. 1b and 1c, both salinity and temperature show minimal variation in STMW, OW, and NPDW, while greater variability is observed in SW and NPIW. This is largely attributed to the processes of air-sea exchange (Liss and Merlivat, 1986) and water mass mixing occurring within these two water masses (Hansell et al., 2002).

Additionally, both DOC and CDOM concentrations displayed significant variability, similar to salinity, particularly in NPIW, indicating distinct mixing characteristics (Figs. 2a, b and S2a, b). In particular, the composition of FDOM varies significantly with depth and water mass, showing substantial differences in relation to DOC concentration as well as the values of $S_{275\text{-}295}$, HIX, and BIX (Figs. 2b and 2g-i). Significant differences exist between the OW and other water masses, resulting in the differences among the other water masses appearing less pronounced (Figs. 2b, 2g-i), which may be attributed to the increased terrestrial-derived DOM associated with OW (Mizuno et al., 2018). Overall, the compositional differences of component C3 across the

various water masses are the smallest. For example, analysis of the fluorescence intensity distribution reveals that component C3 exhibits a more concentrated distribution relative to components C1 and C2 among the three end-member water masses (STMW, OW, and NPDW), as well as the three subcomponents of NPIW, often demonstrating a unimodal distribution, which indicates its relative stability (Fig. S5). Furthermore, among the FDOM components identified in the KOCR samples, only component C3 shows no correlation with any of the dominant microbial genera (Fig. S6), suggesting that C3 lacks biological reactivity. Additionally, compared to C1 and C2, component C3 exhibits a more significant correlation with salinity (Fig. S7), which is associated with its relatively conservative behavior. Therefore, C3 can be considered an alternative end member, alongside neutral density, in mixing models used to distinguish between water masses with similar salinity. The PCA results indicate that CDOM is sensitive to and correlates with traditional physical oceanographic parameters, including temperature, salinity, and γ^n (Fig. S4), suggesting that utilizing the properties of CDOM for water mass classification is feasible. Furthermore, the majority of hydrological and CDOM parameters, along with the PCA results, demonstrate that the characteristics of STMW and NPDW are remarkably similar, making it challenging to distinguish between the two. However, when CDOM parameters are combined with γ^n, the end members of STMW, NPDW, and OW can be effectively differentiated. As illustrated in Fig. 4a, most samples fall within the region defined by the means of the C3 component and γ^n of the three end members. In the end-member mixing model established with γ^n and C3, the NPIW samples are primarily distributed near the mixing line of STMW and OW, or close to the mixing line of NPDW and OW, with very few samples found near the mixing line of STMW and NPDW (Fig. 4a). This indicates that, regardless of the extent of contribution, OW is an indispensable component in the mixing process of NPIW.

The contributions of different water masses to the three subcomponents of NPIW vary significantly. Station D4 is located at the center of water mass mixing, with $NPIW_u$, $NPIW_m$, and $NPIW_l$ distributed above and below this site, extending outward. Overall, the mixing depth on the southern side is greater than that on the northern side (Figs. 4 and 5). At stations D2 and D7, which are farther from D4, $NPIW_u$ is absent, indicating that the primary mixing processes contributing to $NPIW_u$ involve STMW and OW. Correspondingly, $NPIW_l$ is characterized by the upward diffusion of NPDW, while $NPIW_m$ reflects a combination of the aforementioned mixing processes. Previous studies on NPIW have predominantly focused on $NPIW_u$. For instance, research has indicated that $NPIW_u$ is the main region where STMW undergoes cooling and sinking (Suga and Hanawa, 1990; Qu et al., 2002; Oka and Qiu, 2012; Ju et al., 2025). Studies specifically addressing $NPIW_m$ and $NPIW_l$ are limited (Yoshinari et al., 2001). The contribution of NPDW to NPIW, particularly to $NPIW_l$, may be substantial, as evidenced by the relationship between γ^n and C3 (Fig. 4a). Model results also indicate that NPDW accounts for an average of 39% and 78% of $NPIW_m$ and $NPIW_l$, respectively, surpassing the contribution from STMW. At the mixing center, station D4, the deepest boundaries of $NPIW_u$ and $NPIW_m$ are observed, and the influence of NPDW is more pronounced compared to stations on the southern side at the same depth, suggesting that D4 represents a temperature front with significant upwelling and downwelling dynamics (Talley, 1997). Furthermore, microbial analyses also indicate the presence of deep-sea microorganisms associated with NPDW in NPIW. This suggests that previous theories may have underestimated the impact of NPDW on the formation of NPIW.

4.2. Changes of DOM components during the formation of new NPIW

As previously mentioned, different water masses exhibit distinct characteristics of DOM, and the mixing of these water masses can lead to further alterations in DOM properties. The concentration of DOC in NPIW lies between that of STMW and OW and NPDW (Fig. 2a), indicating that this water mass plays a critical role in the transformation of

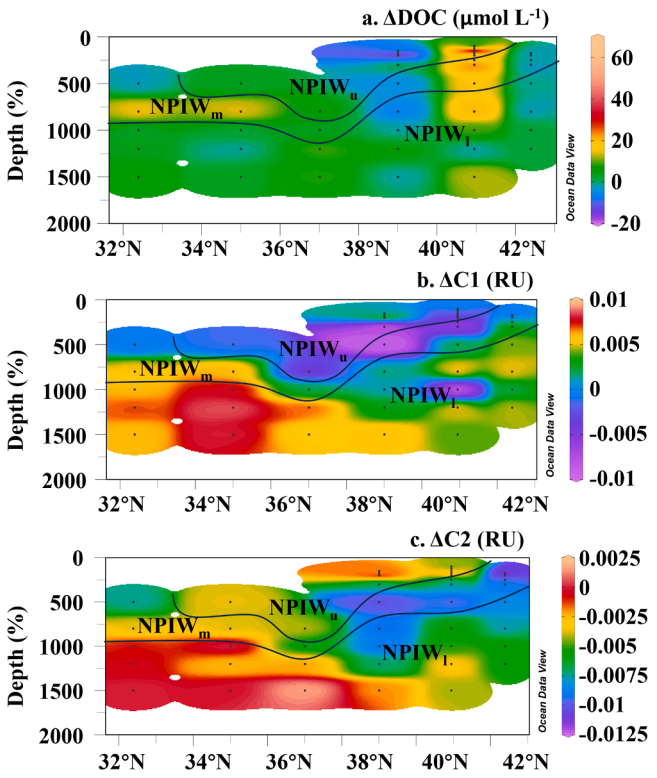

Fig. 5. Profiles of the changes in DOM properties ((a) ΔDOC, (b) ΔC1, and (c) ΔC2) during water mass mixing in the KOCR of the northwest Pacific Ocean. The term "change" refers to the difference between the measured values and the theoretical values calculated based on the water mass proportions. $NPIW_u$, $NPIW_m$ and $NPIW_l$ represent the upper, middle and lower sub-components of NPIW.

DOM. Similar to DOC, the $S_{275\text{-}295}$ generally shows a progressive decrease from surface waters to deeper layers (Fig. 2d), suggesting that the molecular weight of CDOM increases with depth (Cao et al., 2020). This finding aligns with previous research indicating that deep seawater below 1000 meters is characterized by the presence of RDOM with a high molecular weight (Nagata, 2008; Jiao et al., 2011). Influenced by thermohaline circulation, NPDW is also identified as the oldest and least reactive water mass in terms of DOC radiocarbon age and DOM reactivity (Druffel et al., 1992; Medeiros et al., 2015). Notably, the $S_{275\text{-}295}$ values in NPIW are the lowest observed, with some individual samples even lower than those in NPDW (Fig. S2d). This suggests a higher molecular weight of CDOM in NPIW, further indicating that significant DOM transformation occurs during the formation of NPIW, resulting in the production of more HMW-RDOM (Williams and Druffel, 1987; Hansell et al., 2002; Ge et al., 2022). As depth increases, the HIX gradually rises, while the BIX steadily decreases (Figs. 2e and 2f). This trend indicates a higher degree of humification in deeper seawater and lower biological activity. Interestingly, the HIX in NPIW remains the highest, further confirming that the transformation of DOM in this water mass leads to an increased production of recalcitrant compounds. These observations are consistent with the reductions in DOC concentration and $S_{275\text{-}295}$ values (Figs. 2a, 2d, S2a, and S2d), suggesting the accumulation of HMW-RDOM in deeper waters. These findings also align with variations in fluorescent components, particularly C1, and the $SUVA_{254}$ values, indicating the significant accumulation of unsaturated humic-like substances in NPIW and NPDW, as well as the photochemical degradation of such molecules in surface layers (Yamashita et al., 2017; Cao et al., 2020). Overall, the variation in CDOM parameters indicates a transition from smaller, labile molecules to larger, more humified molecules from surface to deeper waters, leading to the accumulation and persistence of RDOM in intermediate to deep waters.

Using the model results as theoretical mixing values, the differences between the measured values of DOC and the FDOM components C1 and C2, as well as their corresponding theoretical values were calculated (Fig. 5). The ΔDOC, ΔC1, and ΔC2 are considered to result from the biogeochemical processes occurring during the mixing of these water masses (Rochelle-Newall and Fisher, 2002; Wang et al., 2021b). The results indicate that ΔDOC does not exhibit significant stratification across the different layers of NPIW, with an average value of 5.2 μmol L^{-1}, although it shows considerable variability, ranging from -13.9 μmol L^{-1} to 64.3 μmol L^{-1} (Fig. 5a). Except for the D4 station, which is influenced by hydrodynamic processes, there is an overall increasing trend, possibly due to the transformation between DOM and particulate OM induced by physical processes in seawater (Digernes et al., 2025). In contrast to ΔDOC, the variations in ΔC1 and ΔC2 are significantly correlated with the stratification of NPIW. Specifically, ΔC1 values from top to bottom in the $NPIW_u$, $NPIW_m$, and $NPIW_l$ layers are -0.15±0.32 × 10^{-2} R.U., -0.00±0.46 × 10^{-2} R.U., and 0.45±0.36 × 10^{-2} R.U., respectively (Fig. 5b). These results indicate that C1 primarily undergoes consumption in the $NPIW_u$ layer and at the boundary between $NPIW_u$ and $NPIW_m$, while accumulation predominates in most of $NPIW_m$ and throughout $NPIW_l$. This reflects the accumulation of RDOM during the formation of NPIW through photodegradation and biodegradation (Hansell, 2013; Medeiros et al., 2015). Conversely, ΔC2 values from top to bottom in the $NPIW_u$, $NPIW_m$, and $NPIW_l$ layers are -0.33±0.21 × 10^{-2} R.U., -0.80±0.25 × 10^{-2} R.U., and -0.38±0.34 × 10^{-2} R.U., respectively (Fig. 5c), indicating that the consumption of C2 occurs at nearly all

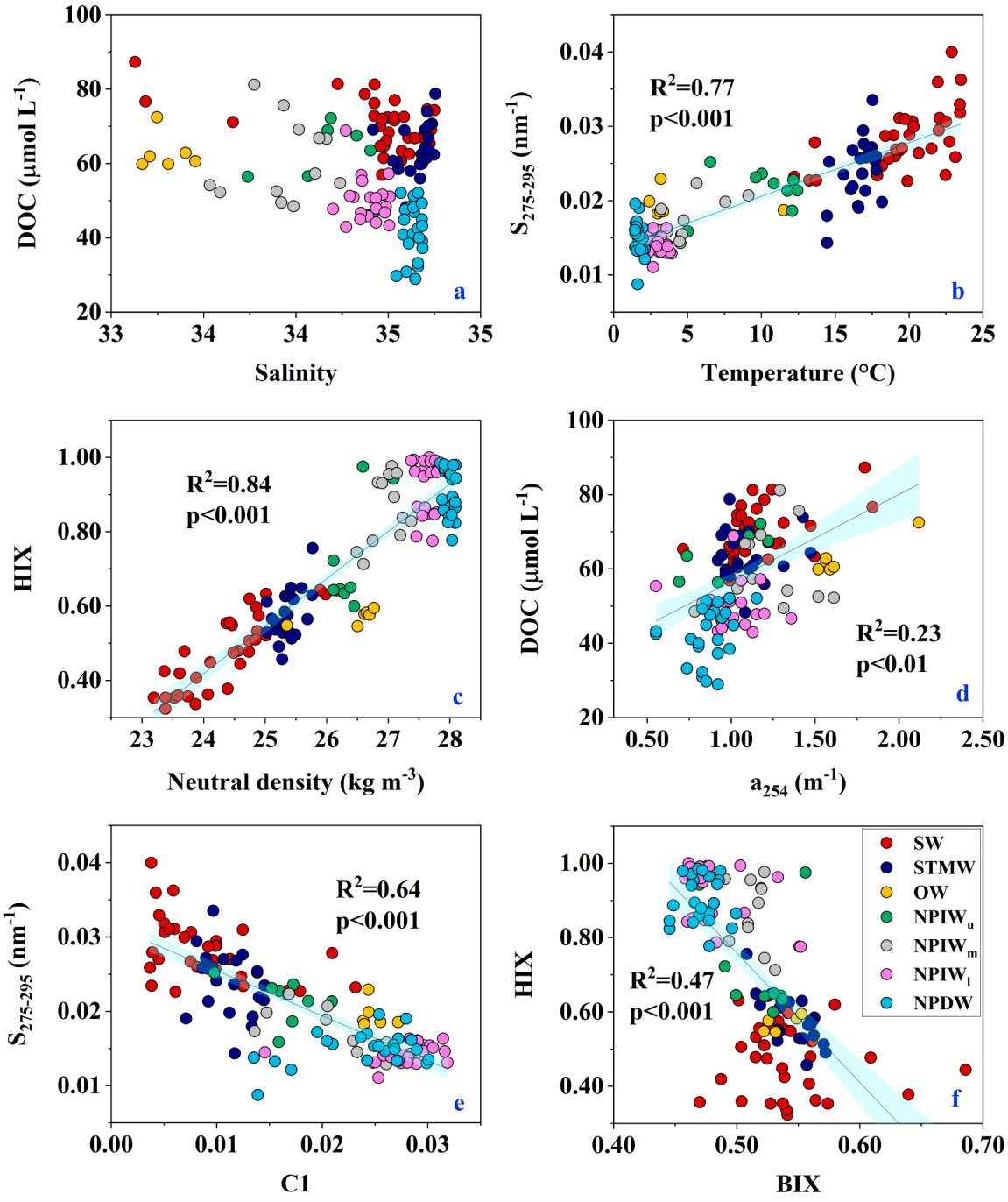

Fig. 6. Scatter plots of (a) salinity vs. DOC, (b) temperature vs. $S_{275\text{-}295}$, (c) neutral density vs. HIX, (d) a_{254} vs. DOC, (e) C1 vs. $S_{275\text{-}295}$, and (f) BIX vs. HIX in the KOCR of the northwest Pacific Ocean.

stations, particularly in $NPIW_m$. The changes in C2 reflect the consumption of labile DOM (LDOM) during the formation of NPIW via biodegradation (Cai et al., 2019; Shen and Benner, 2020; Wang et al., 2021b). Notably, the changes in FDOM components C1 and C2 exhibit a similar trend across all NPIW samples (Fig. 7a), with a clear correlation in $NPIW_u$ and $NPIW_l$, while the correlation in $NPIW_m$ is less pronounced. This discrepancy may be attributed to the more complex mixing processes occurring in $NPIW_m$, which are influenced by both upper and lower water layers (Talley, 1997). This complexity may also contribute to the pronounced consumption of C2 observed in $NPIW_m$. However, there is almost no correlation between ΔC1 and ΔC2 with ΔDOC (Figs. 7b and 7c), suggesting that the variations in DOC concentration in this region may depend more on the interactions between different forms of OC driven by physical processes, while biogeochemical processes dominate the changes in the internal composition of DOM, leading to its inertness (Wang et al., 2022b; Digernes et al., 2025).

The observed changes in DOC and FDOM components in NPIW are consistent with alterations in other CDOM parameters that represent the properties of DOM. Specifically, an increase in the FDOM component C1 is associated with a decrease in the biological reactivity of OM (Fig. 7e). Concurrently, a decrease in component C2 correlates with an increase in the humification of OM (Fig. 7f), further indicating that microbial transformations of DOM facilitate the accumulation of RDOM (Cao et al., 2020; Cai and Jiao, 2024). Collectively, these changes contribute to an increase in the molecular weight of CDOM within the water mass (Fig. 7d), which is characteristic of humic-like substances (Wang et al., 2022b). Following the alterations in NPIW, the characteristics of DOM are ultimately established (Fig. 6), representing a significant mechanism for the preservation of surface-derived OM in intermediate waters (Hansell et al., 2002; Hansell, 2013; Cao et al., 2020).

4.3. Controls on the transformation of DOM during the formation of new NPIW

Hydrological parameters are not the primary factors controlling the changes in the properties of DOM during water mass mixing processes. The KOCR region is a globally significant area for the generation of intermediate water, characterized by the mixing of multiple water masses and various biogeochemical processes (Ge et al., 2022; Hansell et al., 2002). These water masses exhibit significant differences in temperature and salinity, which, like DOM properties, show a gradient change from the surface to the deep layers (Cao et al., 2020; Wang et al., 2022b). However, the relationship between temperature, salinity, and DOM properties is not clearly defined. For instance, the salinity of STMW and NPDW is nearly identical, yet their DOM properties and DOC concentrations differ substantially (Fig. 6a). In this study, samples were collected across a span of 12 degrees latitude and a depth of 4000 meters, revealing significant temperature variations that appear to correlate with certain DOM properties, such as $S_{275\text{-}295}$, which represents molecular weight ($R^2 = 0.77$, $p < 0.001$) (Fig. 6b). NPDW, NPIW, and OW are nearly identical in terms of temperature and molecular weight (Fig. 6b); however, other parameters indicate that these three water masses exhibit notable differences (Figs. 2, 6c, and S2). Furthermore, throughout the study area, there is a general trend of increasing DOM molecular weight and inert material from the surface to the depths, while the concentration of active material gradually decreases (Figs. 2, 6c, 6e). However, the trends are not completely consistent (Figs. 2 and S2), suggesting that different DOM properties respond differently to environmental changes. There is a certain degree of correlation between CDOM content (a_{254}) and DOC concentration ($R^2 = 0.23$, $p < 0.01$) (Fig. 6d), although this correlation is not strong. While DOC concentrations decrease, the reduction in CDOM content is not pronounced, indicating the simultaneous presence of production, transformation, and consumption processes. The comparison of HIX and BIX more clearly illustrates this situation (Fig. 6f). At the surface, sunlight disrupts some humic substances without increasing their biological activity (Medeiros et al., 2015); meanwhile, $NPIW_m$ and $NPIW_u$ show a more pronounced increase in freshness, but a decrease in humification, indicating that this region is a major site for biogeochemical processes involving DOM (Hansell et al., 2002).

Microbial activity may be a key factor in controlling the transformation of DOM during the formation of new NPIW. As previously mentioned, different microbial taxa or their combinations are active in various water masses (Figs. 3 and S3). For instance, *Ca.* Nitrosopelagicus is evidently associated with the influx of the Kuroshio Current (Figs. 3a and S3a), while *Ca.* Nitrosopumilus reflects the influence of the Oyashio Current (Figs. 3c and S3c). There is a notable similarity between the distribution of these microbial taxa and the characteristics of DOM. Dominant groups such as Nitrosopumilaceae, Marine group B, SUP05 and Aegean-169 show significant correlations with parameters such as DOC content, $S_{275\text{-}295}$, HIX and CDOM composition (C1) ($p < 0.001$) (Fig. 8), indicating that these microbial groups may play an important role in the changes in DOM characteristics. In contrast to *Ca.* Nitrosopelagicus and *Ca.* Nitrosopumilus, groups like Nitrosopumilaceae and Marine group B are primarily distributed in deeper water masses, particularly in NPDW and NPIW, where they can decompose DOM or alter its composition, leading to an increase in DOM molecular weight and making it more resistant to degradation (Figs. 8a and 8b) (Reji et al., 2019; Malfertheiner et al., 2022; Garritano et al., 2023). AEGEAN-169 has overlapping distributions with SAR11 but is metabolically distinct, possessing the ability to transport and utilize a wider range of sugars as well as trace metals and thiamine (Getz et al., 2023). The accumulation of RDOM may lead to its decline due to a lack of available OM sources, resulting in lower abundances in waters with higher humic content (C1) (Fig. 8d). Different microbial groups exhibit diverse metabolic pathways, leading to varying impacts on DOM transformation. The Nitrosopumilaceae, which belongs to ammonia-oxidizing archaea (AOA), is primarily associated with deep-sea sponges (Garritano et al., 2023). These archaea possess the ability to produce polysaccharides and polyamines by utilizing energy derived from ammonia oxidation, allowing for transformations within DOM (Cho and Azam, 1988; Reji et al., 2019; Liu et al., 2021; Dugenne et al., 2023). Both *Ca.* Nitrosopumilus and Nitrosopumilaceae are classified as AOA and can utilize organic acids as carbon sources for survival (Qin et al., 2017). Marine group B is capable of degrading OM produced by marine photosynthesis, which includes the expression of genes such as RuBisCO and fructose-bisphosphate aldolase class I, facilitating the formation of humic-like substances rich in carboxyl and aldehyde groups (Malfertheiner et al., 2022). SUP05 contains genes for amino acid transport proteins, enabling the utilization of environmental amino acids and consequently reducing their concentration (Anantharaman et al., 2013). This adaptation allows SUP05 to grow rapidly in the nutrient- and energy-rich layers of $NPIW_m$ and $NPIW_l$, consuming substantial amounts of protein-like substances and increasing the humification state of DOM molecules in these waters (Fig. 8c). In the sub-components of NPIW, the composition of microbial communities exhibits both similarities and differences, which in turn leads to variations in the production and consumption processes of DOM. For instance, Nitrosopumilaceae is present throughout the NPIW, with a slightly higher relative abundance in $NPIW_l$ compared to $NPIW_u$ and $NPIW_m$. Conversely, *Ca.* Nitrosopelagicus is almost absent in $NPIW_l$ and predominantly found in $NPIW_u$ and $NPIW_m$. Marine group B and SUP05 are also present across all NPIW sub-components, but their abundance is significantly higher in $NPIW_m$ and $NPIW_l$ than in $NPIW_u$ (Fig. 3). In $NPIW_u$, although there is some production of C1, both C1 and C2 are primarily consumed due to the activity of microbes such as *Ca.* Nitrosopumilus, resulting in negative values for ΔC1 and ΔC2 (Figs. 5 and 8). In $NPIW_m$, there are microbes that produce C1 (e.g., Nitrosopumilaceae and Marine group B) as well as those that consume C1 and C2 (e.g., *Ca.* Nitrosopumilus and SUP05), with a greater rate of C2 consumption compared to $NPIW_u$ (Fig. 9). In contrast, $NPIW_l$ contains microbes that consume C2 (e.g., SUP05) alongside those that produce C1 and C2 (e.g., Nitrosopumilaceae and Marine group B), with C2

consumption being lower than in $NPIW_m$, while the accumulation of C1 is more pronounced (Figs. 9b, 9e, and 9f). Overall, the synergistic interactions among these microbial communities lead to an increase in the accumulation of RDOM with depth, while the consumption of LDOM is most pronounced in $NPIW_m$. Furthermore, the analysis indicates that NDPW plays a significant role in the transport and transformation of DOM during the formation of NPIW, which should not be overlooked (Fig. 10). During the mixing process, the contribution of microbial communities from deeper waters effectively degrades LDOM and facilitates the accumulation of RDOM.

Microorganisms may facilitate the transformation of DOM during the formation of new NPIW through a phenomenon known as the priming effect. The priming effect refers to significant alterations in the turnover of local OM, particularly recalcitrant one, induced by the addition of exogenous labile OM (Bianchi, 2011). In this study, both STMW and OW contain relatively abundant labile protein-like DOM, while NPDW is rich in humic-like substances that are more recalcitrant. Each of these water masses harbors distinct microbial communities, which create the necessary conditions for the occurrence of a composite priming effect during their mixing. As previously noted, the humic-like C1 component in NPIW does not continuously accumulate; rather, it exhibits a pattern of initial decrease followed by an increase from top to bottom (Fig. 5b). Notably, in NPIW with high mixing intensity, particularly at station D4, there is evidence of simultaneous consumption of both the C1 and labile protein-like C2 components (Figs. 5 and 9). This suggests that the humic-like C1 component may not be entirely non-degradable; the consumption of the active protein-like C2 component could concurrently lead to the degradation of some of the more inert humic-like C1, facilitating its transformation into more recalcitrant DOM. Changes in microbial abundance further support the existence of the priming effect. Specifically, although Nitrosopumilaceae, Marine group B, and SUP05 are all classified as deep-sea microorganisms, the abundance of Marine group B and SUP05 in NPDW is even lower than that in NPIW (Fig. 3). This may indicate that these microbial taxa experience a release from growth limitations upon entering NPIW, or that the conditions in NPIW are more favorable for their reproduction. Consequently, they may proliferate rapidly while converting non-degradable DOM from the upper layers into more inert DOM. This not only indicates the potential existence of the priming effect but also implies that the mixing process of the water masses promotes this transformation (Fig. 10).

It is worth noting that the transformation of DOM in the ocean is influenced not only by microbial activity but also by processes such as chemical oxidation and the adsorption of particulate matter. In the KOCR, the impact of chemical oxidation on DOM transformation has been extensively detailed in previous studies (Wang et al., 2022b), primarily occurring in the upper layer of NPIW, specifically the $NPIW_u$ layer in this study. The negative correlation between ΔC1 and ΔC2 with ΔDOC in the $NPIW_u$ layer may be attributed to chemical oxidation (Fig. 7). However, no significant correlation was observed in the $NPIW_m$ layer and below, suggesting that the influence of chemical oxidation is limited in these regions. In addition, incubation experiments have shown that the processes of adsorption and desorption between particulate OM and DOM typically occur within a timeframe of several hours to days (Digernes et al., 2025), which is considerably shorter than the mixing and circulation times of water masses. Furthermore, the distribution of OC in the ocean differs from that in estuarine and coastal environments, with particulate OC (POC) concentrations being low and significantly below those of DOC, indicating that the processes of dissolution or aggregation have a minimal impact on DOC levels (Zhang et al., 2018).

5. Conclusions

In this study, the transport and transformation processes of DOM during water mass mixing were investigated in the KOCR. It was found that the conservative component of FDOM C3, along with neutral density, can effectively quantify the differentiation of water masses. The residuals between the theoretical mixing values derived from the model and the observed values can be used to examine changes in the properties of DOM during water mass mixing. During the formation of NPIW, potential priming effects and microbial processes may lead to the transformation of DOM into more recalcitrant DOM. Furthermore, besides STMW and OW, NPDW also plays a significant role in the formation of NPIW and the transformation of DOM properties within it. This study contributes to a deeper understanding of the impact of physical mixing processes on the biogeochemical transformation of DOM and

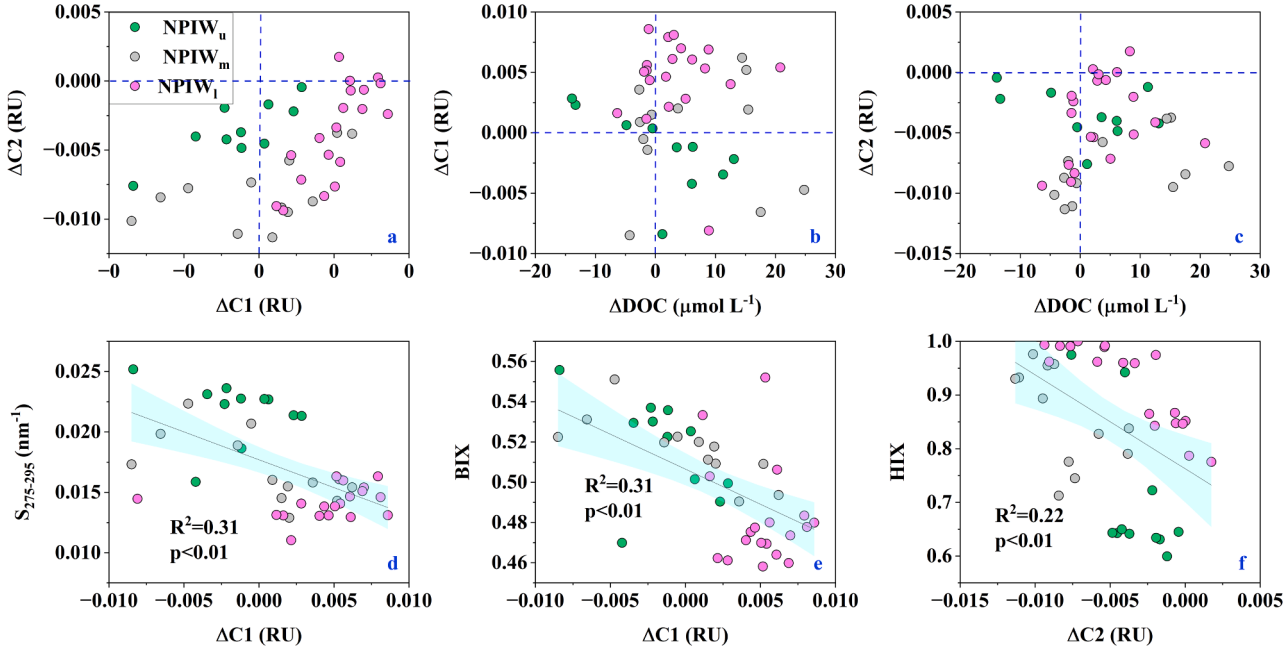

Fig. 7. Scatter plots of (a) ΔC1 vs. ΔC2, (b) ΔDOC vs. ΔC1, (c) ΔDOC vs. ΔC2, (d) ΔC1 vs. $S_{275-295}$, (e) ΔC1 vs. BIX, and (f) ΔC2 vs. HIX in the KOCR of the northwest Pacific Ocean. The green, grey and pink circles represent the samples of the upper, middle and lower sub-components of NPIW ($NPIW_u$, $NPIW_m$ and $NPIW_l$).

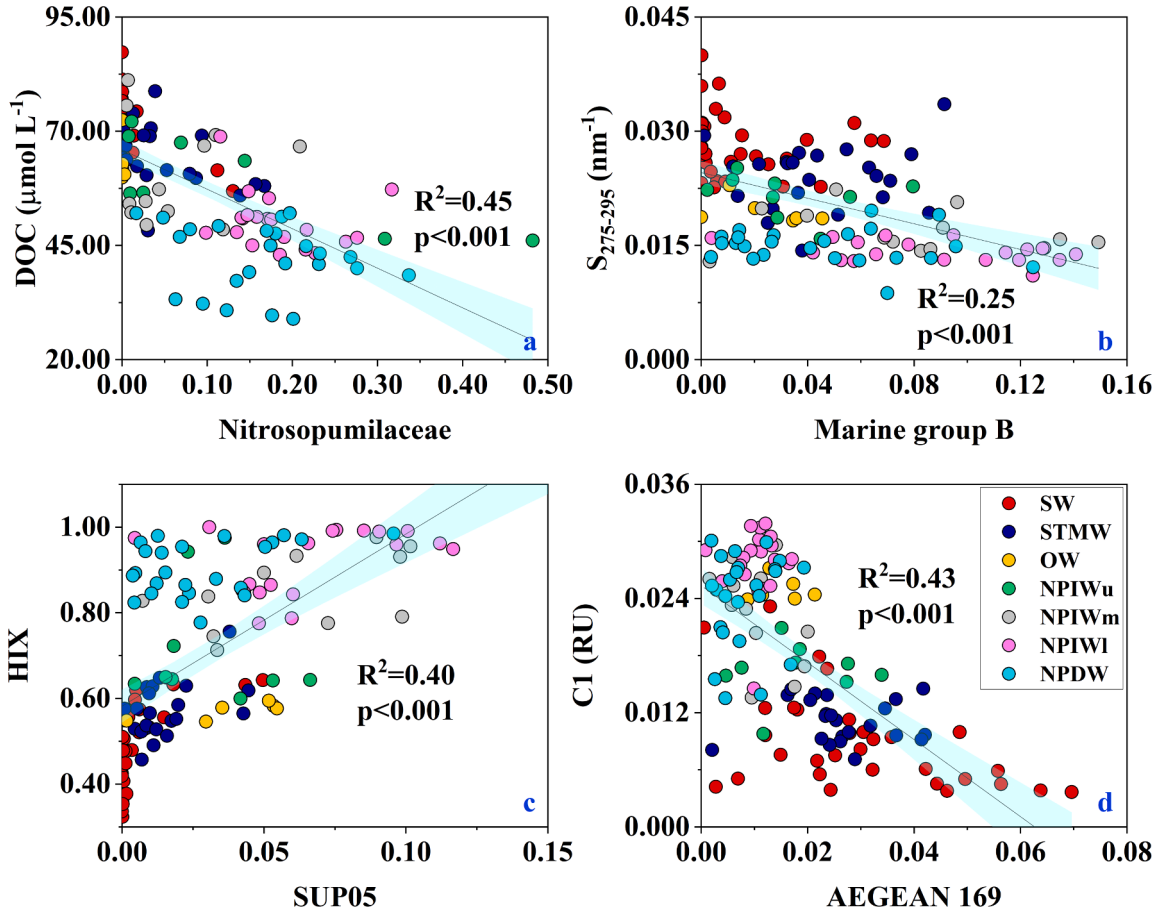

Fig. 8. Relationships of microbial abundance and DOM properties in the KOCR of the northwest Pacific Ocean. (a) Nitrosopumilaceae vs. DOC, (b) Marine group B vs. $S_{275\text{-}295}$, (c) SUP05 vs. HIX, and (d) Aegean-169 vs. C1.

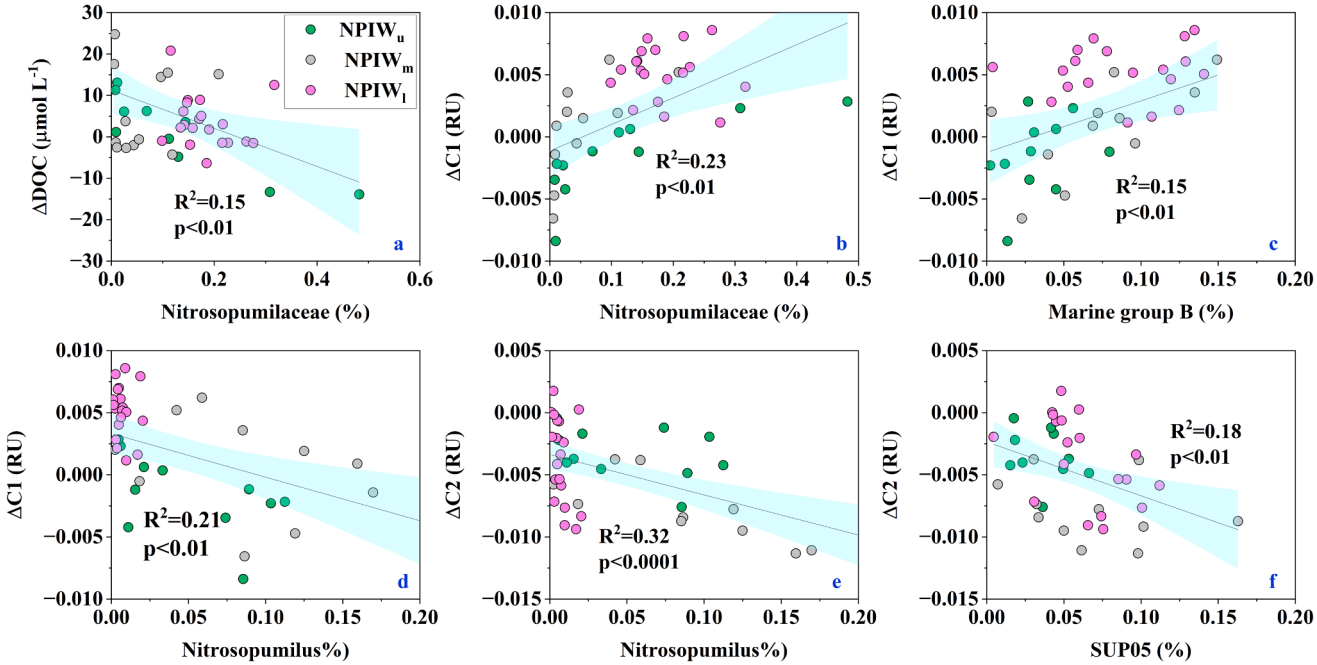

Fig. 9. Relationships of microbial abundance and the changes in DOM properties in the KOCR of the northwest Pacific Ocean. (a) Nitrosopumilaceae vs. ΔDOC, (b) Nitrosopumilaceae vs. ΔC1, (c) Marine group B vs. ΔC1, (d) *Candidatus* Nitrosopumilus vs. ΔC1, (e) *Candidatus* Nitrosopumilus vs. ΔC2, and (f) SUP05 vs. ΔC2. The green, grey and pink circles represent the samples of the upper, middle and lower sub-components of NPIW ($NPIW_u$, $NPIW_m$ and $NPIW_l$).

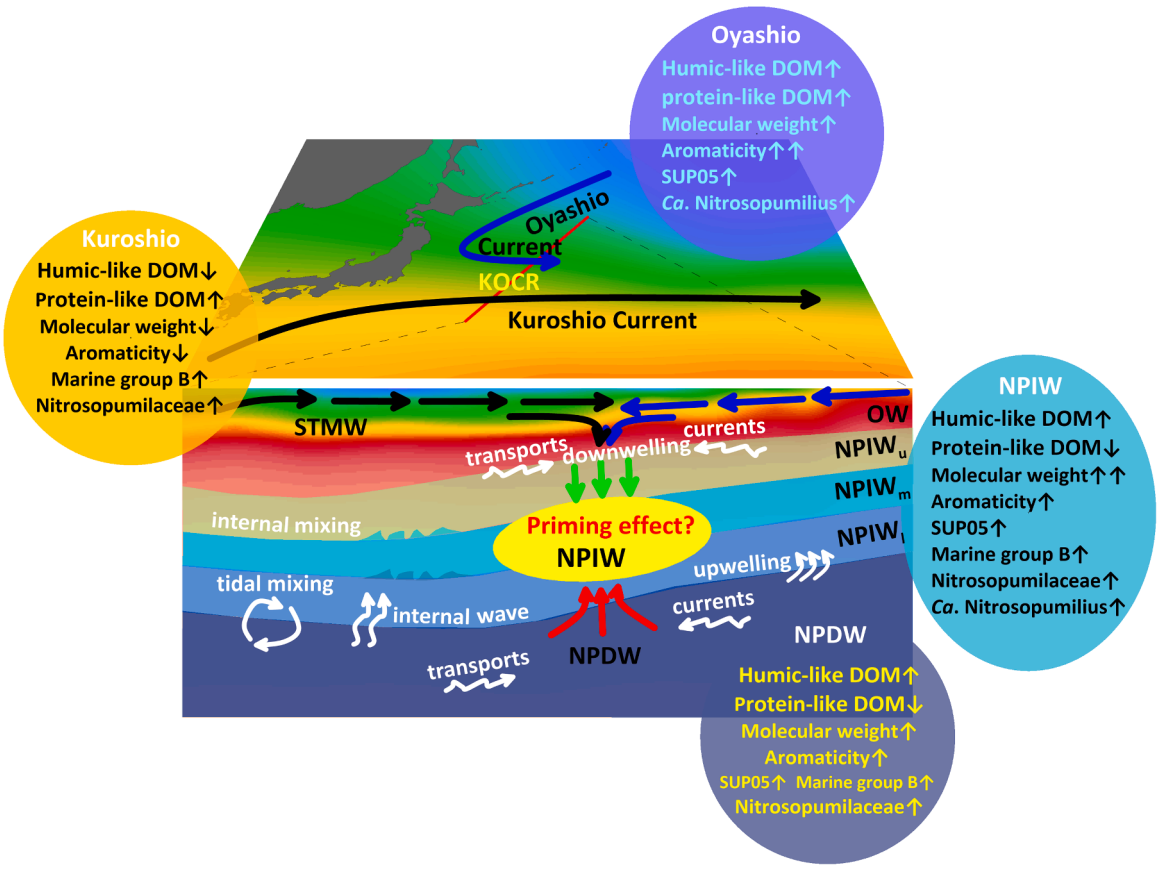

Fig. 10. Conceptual diagram illustrating the changes in DOM properties and the predominant microbial communities during the mixing of water masses and the formation of new NPIW.

aids in the understanding of the formation and persistence mechanisms of RDOM in deep-sea environments.

CRediT authorship contribution statement

Lulu Han: Writing – original draft, Software, Methodology, Investigation, Formal analysis, Data curation, Conceptualization. **Rong Huang:** Methodology, Investigation, Data curation. **Ke Zeng:** Methodology, Data curation. **Xiao-Hua Zhang:** Writing – review & editing, Validation, Supervision, Resources. **Honghai Zhang:** Resources, Investigation. **Zhaohui Chen:** Resources, Funding acquisition. **Peng Yao:** Writing – review & editing, Validation, Supervision, Resources, Project administration, Funding acquisition, Conceptualization.

Declaration of competing interest

The authors declare that they have no known competing financial interests or personal relationships that could have appeared to influence the work reported in this paper.

Acknowledgments

This work was supported by the National Natural Science Foundation of China (42376046) and the Fundamental Research Funds for Central Universities (202072001). We extend our gratitude to Kang Li, Wen Hong, and the crew of the R/V Dongfanghong 3 for their exceptional support in obtaining the samples. We also wish to acknowledge Penghui Li and Chao Wang for their valuable suggestions during the preparation of this manuscript.

Supplementary materials

Supplementary material associated with this article can be found, in the online version, at doi:10.1016/j.watres.2026.125608.

Data availability

Data will be made available on request.

References

Álvarez, E., Cossarini, G., Teruzzi, A., Bruggeman, J., Bolding, K., Ciavatta, S., Vellucci, V., D'Ortenzio, F., Antoine, D., Lazzari, P., 2023. Chromophoric dissolved organic matter dynamics revealed through the optimization of an optical–biogeochemical model in the northwestern Mediterranean Sea. Biogeosciences 20, 4591–4624.

An, S., Chen, F., Chen, S., Feng, M., Jiang, M., Xu, L., Wen, S., Zhang, Q., Xu, J., Du, Y., Zhang, Y., 2023. In-lake processing counteracts the effect of allochthonous input on the composition of color dissolved organic matter in a deep lake. Sci. Total Environ. 856, 158970.

Anantharaman, K., Breier, J.A., Sheik, C.S., Dick, G.J., 2013. Evidence for hydrogen oxidation and metabolic plasticity in widespread deep-sea sulfur-oxidizing bacteria. P. Natl. Acad. Sci. U.S.A. 110 (1), 330–335.

Andersson, A., 2011. A systematic examination of a random sampling strategy for source apportionment calculations. Sci. Total Environ. 412, 232–238.

Andersson, A., Deng, J., Du, K., Zheng, M., Yan, C., Skold, M., Gustafsson, O., 2015. Regionally-varying combustion sources of the January 2013 severe haze events over eastern China. Environ. Sci. Technol. 49 (4), 2038–2043.

Arrieta, J.M., Mayol, E., Hansman, R.L., Herndl, G.J., Dittmar, T., Duarte, C.M., 2015. Dilution limits dissolved organic carbon utilization in the deep ocean. Science 348 (6232), 331–333.

Bianchi, T.S., 2011. The role of terrestrially derived organic carbon in the coastal ocean: a changing paradigm and the priming effect. P. Natl. Acad. Sci. U.S.A. 108 (49), 19473–19481.

Bingham, F.M., Suga, T., Hanawa, K., 1992. Comparison of upper ocean thermal conditions in the western North Pacific between two pentads: 1938–42 and 1978–82. J. Oceanogr. 48, 405–425.

Broecker, W.S., Takahashi, T., Takahashi, T., 1985. Sources and flow patterns of deep-ocean waters as deduced from potential temperature, salinity, and initial phosphate concentration. J. Geophys. Res. Oceans 90 (C4), 6925–6939.
Cai, R., Jiao, N., 2024. Microbial carbon pump shapes chemical signatures of refractory dissolved organic carbon in ocean water column. Sci. China Earth Sci. 5, 2408–2410.
Cai, R., Zhou, W., He, C., Tang, K., Guo, W., Shi, Q., Gonsior, M., Jiao, N., 2019. Microbial processing of sediment-derived dissolved organic matter: Implications for its subsequent biogeochemical cycling in overlying seawater. J. Geophys. Res. Biogeosci. 124, 3479–3490.
Cao, F., Zhu, Y., Kieber, D.J., Miller, W.L., 2020. Distribution and photo-reactivity of chromophoric and fluorescent dissolved organic matter in the Northeastern North Pacific Ocean. Deep Sea Res. I. 155, 103168.
Catalá, T.S., Álvarez-Salgado, X.A., Otero, J., Iuculano, F., Companys, B., Horstkotte, B., Romera-Castillo, C., Nieto-Cid, M., Latasa, M., Morán, X.A.G., Gasol, J.M., Marrasé, C., Stedmon, C.A., Reche, I., 2016. Drivers of fluorescent dissolved organic matter in the global epipelagic ocean. Limnol. Oceanogr. 61, 1101–1119.
Catalá, T.S., Reche, I., Fuentes-Lema, A., Romera-Castillo, C., Nieto-Cid, M., Ortega-Retuerta, E., Calvo, E., Álvarez, M., Marrasé, C., Stedmon, C.A., Álvarez-Salgado, X. A., 2015. Turnover time of fluorescent dissolved organic matter in the dark global ocean. Nat. Commun. 6, 5986.
Chang, F.H., Gong, G.C., Hsieh, C.H., Chen, W.Y., Mukhanov, V., Tsai, A.Y., 2024. Vertical variations of bacterial growth, mortality loss to nanoflagellates, and viruses in the subtropical northwestern Pacific Ocean. J. Mar. Syst. 243, 103963.
Chen, M., Jung, J., Lee, Y.K., Kim, T.W., Hur, J., 2019. Production of tyrosine-like fluorescence and labile chromophoric dissolved organic matter (DOM) and low surface accumulation of low molecular weight-dominated DOM in a productive Antarctic sea. Mar. Chem. 213, 40–48.
Chen, R.F., Gardner, G.B., 2004. High-resolution measurements of chromophoric dissolved organic matter in the Mississippi and Atchafalaya River plume regions. Mar. Chem. 89, 103–125.
Cho, B.C., Azam, F., 1988. Major role of bacteria in biogeochemical fluxes in the ocean's interior. Nature 332, 441–443.
D'Andrilli, J., Silverman, V., Buckley, S., Rosario-Ortiz, F.L., 2022. Inferring ecosystem function from dissolved organic matter optical properties: A critical review. Environ. Sci. Technol. 56, 11146–11161.
Digernes, M.G., Bodur, Y.V., Amargant-Arumí, M., Müller, O., Hawkes, J.A., Kohler, S.G., Dietrich, U., Reigstad, M., Paulsen, M.L., 2025. Contrasting seasonal patterns in particle aggregation and dissolved organic matter transformation in a sub-arctic fjord. Biogeosciences 22 (2), 601–623.
Ding, L., Ge, T., Gao, H., Luo, C., Xue, Y., Druffel, E.R.M., Wang, X., 2018. Large variability of dissolved inorganic radiocarbon in the Kuroshio Extension of the Northwest North Pacific. Radiocarbon 60, 691–704.
Dittmar, T., Lennartz, S.T., Buck-Wiese, H., Hansell, D.A., Santinelli, C., Vanni, C., Blasius, B., Hehemann, J.H., 2021. Enigmatic persistence of dissolved organic matter in the ocean. Nat. Rev. Earth Environ. 2 (8), 570–583.
Druffel, E.R.M., Williams, P.M., Bauer, J.E., Ertel, J.R., 1992. Cycling of dissolved and particulate organic matter in the open ocean. J. Geophys. Res. 97, 15639.
D'Sa, E.J., Goes, J.I., Gomes, H., Mouw, C., 2014. Absorption and fluorescence properties of chromophoric dissolved organic matter of the eastern Bering Sea in the summer with special reference to the influence of a cold pool. Biogeosciences 11, 3225–3244.
Dugenne, M., Gradoville, M.R., Church, M.J., Wilson, S.T., Sheyn, U., Harke, M.J., Bjrkman, K.M., Hawco, N.J., Hynes, A.M., Ribalet, F., 2023. Nitrogen fixation in mesoscale eddies of the North Pacific Subtropical Gyre: Patterns and mechanisms. Global Biogeochem. Cy. 37 (4) e2022GB007386.
Gan, B., Wang, T., Wu, L., Li, J., Qiu, B., Yang, H., Zhang, L., 2023. A mesoscale ocean–atmosphere coupled pathway for decadal variability of the Kuroshio extension system. J. Clim. 36, 485–510.
Ganachaud, A., 2003. Large-scale mass transports, water mass formation, and diffusivities estimated from World Ocean Circulation Experiment (WOCE) hydrographic data. J. Geophys. Res. Oceans 108, 3211.
Garritano, A.N., Majzoub, M.E., Ribeiro, B., Damasceno, T., Modolon, F., Messias, C., Vilela, C., Duarte, G., Hill, L., Peixoto, R., Thomas, T., 2023. Species-specific relationships between deep sea sponges and their symbiotic Nitrosopumilaceae. ISME J. 17, 1517–1519.
Ge, T., Luo, C., Ren, P., Zhang, H., Chen, H., Chen, Z., Zhang, J., Wang, X., 2022. Dissolved organic carbon along a meridional transect in the western North Pacific Ocean: Distribution, variation and controlling processes. Front. Mar. Sci. 9, 909148.
Getz, E.W., Lanclos, V.C., Kojima, C.Y., Cheng, C., Henson, M.W., Schön, M.E., Ettema, T. J.G., Faircloth, B.C., Thrash, J.C., 2023. The AEGEAN-169 clade of bacterioplankton is synonymous with SAR11 subclade V (HIMB59) and metabolically distinct. Msystems 8 e00179–23.
Gomez-Letona, M., Sebastián, M., Baños, I., Montero, M.F., Barrancos, C.P., Baumann, M., Riebesell, U., Arístegui, J., 2022. The importance of the dissolved organic matter pool for the carbon sequestration potential of artificial upwelling. Front. Mar. Sci. 9, 969714.
Gonçalves-Araujo, R., Granskog, M.A., Bracher, A., Azetsu-Scott, K., Dodd, P.A., Stedmon, C.A., 2016. Using fluorescent dissolved organic matter to trace and distinguish the origin of Arctic surface waters. Sci. Rep. 6, 33978.
Gong, X., Lembke-Jene, L., Lohmann, G., Knorr, G., Tiedemann, R., Zou, J.J., Shi, X.F, 2019. Enhanced North Pacific deep-ocean stratification by stronger intermediate water formation during Heinrich Stadial 1. Nat. Commun. 10 (1), 656.
Guéguen, C., Cuss, C.W., Cassels, C.J., Carmack, E.C., 2014. Absorption and fluorescence of dissolved organic matter in the waters of the Canadian Arctic Archipelago, Baffin Bay, and the Labrador Sea. J. Geophys. Res. Oceans 119, 2034–2047.
Guo, L., Santschi, P.H., Warnken, K.W., 1995. Dynamics of dissolved organic carbon (DOC) in oceanic environments. Limnol. Oceanogr. 40, 1392–1403.
Hansell, D.A., Carlson, C.A., 2013. Localized refractory dissolved organic carbon sinks in the deep ocean. Global Biogeochem. Cy. 27, 705–710.
Hansell, D.A., 2013. Recalcitrant dissolved organic carbon fractions. Annu. Rev. Mar. Sci. 5, 421–445.
Hansell, D.A., Carlson, C.A., Suzuki, Y., 2002. Dissolved organic carbon export with North Pacific Intermediate Water formation. Global Biogeochem. Cy. 16 (1), 1007.
Hansell, D.A., Carlson, C.A., Repeta, D.J., Schlitzer, R., 2009. Dissolved organic matter in the ocean a controversy stimulates new insights. Oceanography 22, 202–211.
Helms, J.R., Stubbins, A., Ritchie, J.D., Minor, E.C., Kieber, D.J., Mopper, K., 2008. Absorption spectral slopes and slope ratios as indicators of molecular weight, source, and photobleaching of chromophoric dissolved organic matter. Limnol. Oceanogr. 53, 955–969.
Hirawake, T., Oida, J., Yamashita, Y., Waga, H., Abe, H., Nishioka, J., Nomura, D., Ueno, H., Ooki, A., 2021. Water mass distribution in the northern Bering and southern Chukchi seas using light absorption of chromophoric dissolved organic matter. Prog. Oceanogr. 197, 102856.
Huang, R., Zhang, Y., Han, L., Liu, R., Zhai, X., Zeng, K., Song, G., Zhang, H., Yao, P., Chen, Z., Liu, J., Zhang, X.H., 2026. From currents to water masses: fine-scale insights into microbial biogeography in the Kuroshio–Oyashio Extension region. Appl. Environ. Microb. 92 (1) e01960-25.
Huguet, A., Vacher, L., Relexans, S., Saubusse, S., Froidefond, J.M., Parlanti, E., 2009. Properties of fluorescent dissolved organic matter in the Gironde Estuary. Org. Geochem. 40, 706–719.
Jackett, D.R., Mcdougall, T.J., 1997. A neutral density variable for the world's oceans. J. Phys. Oceanogr. 27, 237–263.
Jiao, N., Herndl, G.J., Hansell, D.A., Benner, R., Kattner, G., Wilhelm, S.W., Kirchman, D. L., Weinbauer, M.G., Luo, T., Chen, F., Azam, F., 2011. The microbial carbon pump and the oceanic recalcitrant dissolved organic matter pool. Nat. Rev. Microbiol. 9, 555.
Jiao, N., Robinson, C., Azam, F., Thomas, H., Baltar, F., Dang, H., Hardman-Mountford, N.J., Johnson, M., Kirchman, D.L., Koch, B.P., Legendre, L., Li, C., Liu, J., Luo, T., Luo, Y.-W., Mitra, A., Romanou, A., Tang, K., Wang, X., Zhang, C., Zhang, R., 2014. Mechanisms of microbial carbon sequestration in the ocean– future research directions. Biogeosciences 11, 5285–5306.
Ju, W.S., Zhang, Y., Du, Y., 2025. Two pathways switch of the North Pacific Eastern Subtropical Mode Water toward the equatorial region identified in sigma-pi distance metric. Clim. Dyn. 63, 66.
Kakehi, S., Ito, S.I., Wagawa, T., 2017. Estimating surface water mixing ratios using salinity and potential alkalinity in the Kuroshio-Oyashio mixed water regions. J. Geophys. Res. Oceans 122, 1927–1942.
Kang, J., Wang, Y., Huang, S., Pei, L., Luo, Z., 2022. Impacts of mesoscale eddies on biogeochemical variables in the Northwest Pacific. J. Mar. Sci. Eng. 10, 1451.
Kim, J., Song, B.C., Kim, T.H., 2022. Origin of dissolved organic carbon under phosphorus-limited coastal-bay conditions revealed by fluorescent dissolved organic matter. Front. Mar. Sci. 9, 971550.
Kothawala, D.N., Stedmon, C.A., Müller, R.A., Weyhenmeyer, G.A., Köhler, S.J., Tranvik, L.J., 2014. Controls of dissolved organic matter quality: evidence from a large-scale boreal lake survey. Glob. Change Biol. 20, 1101–1114.
Lawaetz, A.J., Stedmon, C.A., 2009. Fluorescence intensity calibration using the Raman scatter peak of water. Appl. Spectrosc. 63, 936–940.
Lechtenfeld, O.J., Kattner, G., Flerus, R., McCallister, S.L., Schmitt-Kopplin, P., Koch, B. P., 2014. Molecular transformation and degradation of refractory dissolved organic matter in the Atlantic and Southern Ocean. Geochim. Cosmochim. Acta 126, 321–337.
Letscher, R.T., Wang, W.L., Liang, Z., Knapp, A.N., 2022. Regionally variable contribution of dissolved organic phosphorus to marine annual net community production. Global Biogeochem. Cy. 36 e2022GB007354.
Liss, P.L., Merlivat, L., 1986. Air-sea gas exchange rates: Introduction and synthesis. In: Buat-Ménard, P. (Ed.), The Role of Air-Sea Exchange in Geochemical Cycling. Springer, pp. 113–127.
Liu, L., Liu, M., Jiang, Y., Lin, W., Luo, J., 2021. Production and excretion of polyamines to tolerate high ammonia, a case study on soil ammonia-oxidizing archaeon "Candidatus Nitrosocosmicus agrestis. Msystems 6 (1), 10–1128.
Liu, Z., Cai, R., Chen, Y.L., Zhuo, X., He, C., Zheng, Q., He, D., Shi, Q., Jiao, N., 2023. Direct production of bio-recalcitrant carboxyl-rich alicyclic molecules evidenced in a bacterium-induced steroid degradation experiment. Microbiol. Spectr. 11 e04693-22.
Long, Y., Zhu, X.H., Guo, X., 2019. The Oyashio nutrient stream and its nutrient transport to the mixed water region. Geophys. Res. Lett. 46, 5191–5200.
Long, Y., Zhu, X.H., Guo, X., Huang, H., 2018. Temporal variation of Kuroshio nutrient stream south of Japan. J. Geophys. Res. Oceans 123, 8132–8149.
Malfertheiner, L., Martínez-Pérez, C., Zhao, Z., Herndl, G.J., Baltar, F., 2022. Phylogeny and metabolic potential of the candidate phylum SAR324. Biology 11, 599.
Martínez-Pérez, A.M., Nieto-Cid, M., Osterholz, H., Catalá, T.S., Reche, I., Dittmar, T., Álvarez-Salgado, X.A., 2017. Linking optical and molecular signatures of dissolved organic matter in the Mediterranean Sea. Sci. Rep. 7, 3436.
Masujima, M., Yasuda, I., 2009. Distribution and modification of North Pacific intermediate water around the subarctic frontal zone east of 150°E. J. Phys. Oceanogr. 39, 1462–1474.
Masunaga, E., Uchiyama, Y., Yamazaki, H., 2019. Strong internal waves generated by the interaction of the Kuroshio and tides over a shallow ridge. J. Phys. Oceanogr. 49 (11), 2917–2934.
Matsuoka, A., Babin, M., Devred, E.C., 2016. A new algorithm for discriminating water sources from space: a case study for the southern Beaufort Sea using MODIS ocean color and SMOS salinity data. Remote Sens. Environ. 184, 124–138.

Matsuoka, A., Bricaud, A., Benner, R., Para, J., Sempéré, R., Prieur, L., Bélanger, S., Babin, M., 2012. Tracing the transport of colored dissolved organic matter in water masses of the Southern Beaufort Sea: relationship with hydrographic characteristics. Biogeosciences 9, 925–940.
Medeiros, P.M., Seidel, M., Powers, L.C., Dittmar, T., Hansell, D.A., Miller, W.L., 2015. Dissolved organic matter composition and photochemical transformations in the northern North Pacific Ocean. Geophys. Res. Lett. 42, 863–870.
Meilleur, C., Kamula, M., Kuzyk, Z.A., Guéguen, C., 2023. Insights into surface circulation and mixing in James Bay and Hudson Bay from dissolved organic matter optical properties. J. Mar. Syst. 238, 103841.
Mizuno, Y., Nishioka, J., Tanaka, T., Tada, Y., Suzuki, K., Tsuzuki, Y., Sugimoto, A., Yamashita, Y., 2018. Determination of the freshwater origin of Coastal Oyashio Water using humic-like fluorescence in dissolved organic matter. J. Oceanogr. 74, 509–521.
Murphy, K.R., Hambly, A., Singh, S., Henderson, R.K., Baker, A., Stuetz, R., Khan, S.J., 2011. Organic matter fluorescence in municipal water recycling schemes: Toward a unified PARAFAC model. Environ. Sci. Technol. 45, 2909–2916.
Murphy, K.R., Stedmon, C.A., Wenig, P., Bro, R., 2014. OpenFluor–an online spectral library of auto-fluorescence by organic compounds in the environment. Anal. Methods 6 (3), 658–661.
Nagata, T., 2008. Organic matter–bacteria interactions in seawater. In: Kirchman, D.L. (Ed.), Microbial Ecology of the Oceans. Wiley, pp. 207–241.
Ohno, T., 2002. Fluorescence inner–filtering correction for determining the humification index of dissolved organic matter. Environ. Sci. Technol. 36, 742–746.
Oka, E., Qiu, B., 2012. Progress of North Pacific Mode Water research in the past decade. J. Oceanogr. 68, 5–20.
Qin, W., Heal, K.R., Ramdasi, R., Kobelt, J.N., Martens-Habbena, W., Bertagnolli, A.D., Amin, S.A., Walker, C.B., Urakawa, H., Könneke, M., Devol, H., Moffett, J.W., Armbrust, E.V., Jensen, G.J., Ingalls, A.E., Stahl, D.A., 2017. Nitrosopumilus maritimus gen. nov., sp. nov., Nitrosopumilus cobalaminigenes sp. nov., Nitrosopumilus oxyclinae sp. nov., and Nitrosopumilus ureiphilus sp. nov., four marine ammonia-oxidizing archaea of the phylum Thaumarchaeota. Int. J. Syst. Evol. Microbiol. 67 (12), 5067–5079.
Qu, T., Xie, S.P., Mitsudera, H., Ishida, A., 2002. Subduction of the North Pacific Mode Waters in a global high-resolution GCM. J. Phys. Oceanogr. 32, 746–763.
Reji, L., Tolar, B.B., Smith, J.M., Chavez, F.P., Francis, C.A., 2019. Differential co-occurrence relationships shaping ecotype diversification within Thaumarchaeota populations in the coastal ocean water column. ISME J. 13, 1144–1158.
Rochelle-Newall, E.J., Fisher, T.R., 2002. Production of chromophoric dissolved organic matter fluorescence in marine and estuarine environments: An investigation into the role of phytoplankton. Mar. Chem. 77, 7–21.
Sabine, C.L., Feely, R.A., Gruber, N., Key, R.M., Lee, K., Bullister, J.L., Wanninkhof, R., Wong, C.S., Wallace, D.W.R., Tilbrook, B., Millero, F.J., Peng, T.H., Kozyr, A., Ono, T., Riosand, A.F., 2004. The oceanic sink for anthropogenic CO_2. Science 305, 367–371.
Shen, Y., Benner, R., 2020. Molecular properties are a primary control on the microbial utilization of dissolved organic matter in the ocean. Limnol. Oceanogr. 65, 1061–1071.
Shields, M., Bianchi, T., Osburn, C.L., Kinsey, J., Corradino, G., 2019. Linking chromophoric organic matter transformation with biomarker indices in a marine phytoplankton growth and degradation experiment. Mar. Chem. 214, 103671.
Shin-ichi, Ito, Shigeho, Kakehi, Taku, & Wagawa, 2017. Estimating surface water mixing ratios using salinity and potential alkalinity in the Kuroshio-Oyashio mixed water regions. J. Geophys. Res. Oceans 122 (3), 1927–1942.
Sonnerup, R.E., Quay, P.D., Bullister, J.L., 1999. Thermocline ventilation and oxygen utilization rates in the subtropical North Pacific based on CFC distributions during WOCE. Deep Sea Res. I 46, 777–805.
Spencer, R.G., Coble, P.G., 2014. Sampling design for organic matter fluorescence analysis. In: Coble, P.G., Lead, J., Baker, A., Spencer, R.M.W. (Eds.), Aquatic Organic Matter Fluorescence. Cambridge University Press, pp. 125–146.
Suga, T., Hanawa, K., 1990. The mixed-layer climatology in the northwestern part of the North Pacific subtropical gyre and the formation area of subtropical mode water. J. Mar. Res. 48, 543–566.
Swan, C.M., Siegel, D.A., Nelson, N.B., Carlson, C.A., Nasir, E., 2009. Biogeochemical and hydrographic controls on chromophoric dissolved organic matter distribution in the Pacific Ocean. Deep Sea Res. I 56, 2175–2192.
Takahashi, T., Sutherland, S.C., Wanninkhof, R., Sweeney, C., Feely, R.A., Chipman, D. W., Hales, B., Friederich, G., Chavez, F., Sabine, C., Watson, A., Bakker, D.C.E., Schuster, U., Metzl, N., Yoshikawa-Inoue, H., Ishii, M., Midorikawa, T., Nojiri, Y., Kortzinger, A., Steinhoff, T., Hoppema, M., Olafsson, J., Arnarson, T.S., Tilbrook, B., Johannessen, T., Olsen, A., Bellerby, R., Wong, C.S., Delille, B., Bates, N.R., de Baar, H.J.W., 2009. Climatological mean and decadal change in surface ocean pCO_2, and net sea-air CO_2 flux over the global oceans. Deep Sea Res. II 56, 554–577.
Talley, L.D., 1997. North Pacific intermediate water transports in the mixed water region. J. Phys. Oceanogr. 27, 1795–1803.
Talley, L.D., 2011. Global circulation and water properties. In: Talley, L.D., Pickard, G.L., Emery, W.J., Swift, J.H. (Eds.), Descriptive Physical Oceanography. Academic Press, pp. 1–9.
Tanaka, K., Takesue, N., Nishioka, J., Kondo, Y., Ooki, A., Kuma, K., Hirawake, T., Yamashita, Y., 2016. The conservative behavior of dissolved organic carbon in surface waters of the southern Chukchi Sea, Arctic Ocean, during early summer. Sci. Rep. 6, 34123.
Wang, C., Guo, W., Li, Y., Dahlgren, R.A., Guo, X., Qu, L., Zhuang, W., 2021a. Temperature-regulated turnover of chromophoric dissolved organic matter in global dark marginal basins. Geophys. Res. Lett. 48 e2021GL094035.
Wang, C., Li, Y., Li, Y., Zhou, H., Stubbins, A., Dahlgren, R.A., Wang, Z., Guo, W., 2021b. Dissolved organic matter dynamics in the epipelagic Northwest Pacific Low-Latitude Western Boundary Current System: insights from optical analyses. J. Geophys. Res. Oceans 126 e2021JC017458.
Wang, T., Suga, T., Kouketsu, S., 2022a. Spiciness anomalies in the upper North Pacific based on argo observations. Front. Mar. Sci. 9, 1006042.
Wang, Y., Wang, Y., Ge, H., Liu, B., Wu, J., Han, L., Liu, Y., Yu, J., Xu, Y., 2022b. Optical characterization of dissolved organic matter in Kuroshio-Oyashio confluence region: Implication for water mass mixing. Deep Sea Res. I 185, 103807.
Weishaar, J.L., Aiken, G.R., Bergamaschi, B.A., Fram, M.S., Fujii, R., Mopper, K., 2003. Evaluation of specific ultraviolet absorbance as an indicator of the chemical composition and reactivity of dissolved organic carbon. Environ. Sci. Technol. 37, 4702–4708.
Williams, P.M., Druffel, E.R.M., 1987. Radiocarbon in dissolved organic matter in the central North Pacific Ocean. Nature 330, 246–248.
Xia, F., Liu, Z., Zhao, M., Li, Q., Li, D., Cao, W., Zeng, C., Hu, Y., Chen, B., Bao, Q., Zhang, Y., He, Q., Lai, C., He, X., Ma, Z., Han, Y., He, H., 2022. High stability of autochthonous dissolved organic matter in karst aquatic ecosystems: evidence from fluorescence. Water Res 220, 118723.
Xiao, X., Yamashita, Y., Gonsior, M., Jiao, N., 2023. The efficiency of the microbial carbon pump as seen from the relationship between apparent oxygen utilization and fluorescent dissolved organic matter. Prog. Oceanogr. 210, 102929.
Yamashita, Y., Tanoue, E., 2008. Production of bio-refractory fluorescent dissolved organic matter in the ocean interior. Nat. Geoscience 1 (9), 579–582.
Yamashita, Y., Tanoue, E., 2009. Basin scale distribution of chromophoric dissolved organic matter in the Pacific Ocean. Limnol. Oceanogr. 54, 598–609.
Yamashita, Y., Hashihama, F., Saito, H., Fukuda, H., Ogawa, H., 2017. Factors controlling the geographical distribution of fluorescent dissolved organic matter in the surface waters of the Pacific Ocean. Limnol. Oceanogr. 62, 2360–2374.
Yamashita, Y., Yagi, Y., Ueno, H., Ooki, A., Hirawake, T., 2019. Characterization of the water masses in the shelf region of the Bering and Chukchi Seas with fluorescent organic matter. J. Geophys. Res. Oceans 124, 7545–7556.
Yang, H., Qiu, B., Chang, P., Wu, L., Wang, S., Chen, Z., Yang, Y., 2018. Decadal variability of eddy characteristics and energetics in the Kuroshio Extension: Unstable versus stable states. J. Geophys. Res. Oceans 123, 6653–6669.
Yao, P., Yu, Z., Bianchi, T.S., Guo, Z., Zhao, M., Knappy, C.S., Keely, B.J., Zhao, B., Zhang, T., Pan, H., Wang, J., Li, D., 2015. A multiproxy analysis of sedimentary organic carbon in the Changjiang Estuary and adjacent shelf. J. Geophys. Res. Biogeosci. 120, 1407–1429.
Yasuda, I., Okuda, K., Shimizu, Y., 1996. Distribution and modification of North Pacific Intermediate Water in the Kuroshio-Oyashio interfrontal zone. J. Phys. Oceanogr. 26, 448–465.
Yoshinari, H., Yasuda, I., Ito, S.I., Firing, E., Matsuo, Y., Katoh, O., Shimizu, Y., 2001. Meridional transport of the North Pacific Intermediate Water in the Kuroshio-Oyashio interfrontal zone. Geophys. Res. Lett. 28, 3445–3448.
Zhang, C.L., Dang, H.Y., Azam, F., Benner, R., Legendre, L., Passow, U., Polimene, L., Robinson, C., Suttle, C.A., Jiao, N.Z., 2018. Evolving paradigms in biological carbon cycling in the ocean. Natl. Sci. Rev. 5 (4), 481–499.
Zhao, B., Yao, P., Bianchi, T.S., Yu, Z.G., 2021. Controls on organic carbon burial in the eastern China marginal seas: a regional synthesis. Global Biogeochem. Cy. 35 (4) e2020GB006608.
Zhao, H., Zhang, Z., Nair, S., Li, H., He, C., Shi, Q., Zheng, Q., Cai, R., Luo, G., Xie, S., Jiao, N., Zhang, Y., 2024. Overlooked vital role of persistent algae-bacteria interaction in ocean recalcitrant carbon sequestration and its response to ocean warming. Glob. Change Biol. 30, e17345.